

AI

NASA

NATIONAL AERONAUTICS AND SPACE ADMINISTRATION

NASA APOLLO PROGRAM WORKING PAPER NC. 1325

FRACTURE MECHANICS ANALYSIS OF APOLLO  
BLOCK I TITANIUM ALLOY PRESSURE VESSELS  
(COMMAND AND SERVICE MODULES)

FACILITY FORM 602

<u>N70-34510</u>	(HRU)
(ACCESSION NUMBER)	
<u>50</u>	(CODE)
(PAGES)	
<u>TMX-64391</u>	<u>32</u>
(NASA CR OR TMX OR AD NUMBER)	(CATEGORY)



MANNED SPACECRAFT CENTER  
HOUSTON, TEXAS

February 1967

NASA APOLLO PROGRAM WORKING PAPER NO. 1325

FRACTURE MECHANICS ANALYSIS OF APOLLO  
BLOCK I TITANIUM ALLOY PRESSURE VESSELS  
(COMMAND AND SERVICE MODULES)

PREPARED BY

*S. V. Glorioso*

---

S. V. Glorioso  
AST, Materials Technology Branch

*G. M. Ecord*

---

G. M. Ecord  
AST, Materials Technology Branch

AUTHORIZED FOR DISTRIBUTION

*Warren Gillespie, Jr.*

---

for Maxime A. Fagot  
Director of Engineering and Development

NATIONAL AERONAUTICS AND SPACE ADMINISTRATION

MANNED SPACECRAFT CENTER

HOUSTON, TEXAS

February , 1967

PRECEDING PAGE BLANK NOT FILMED.

iii

CONTENTS

Section	Page
SUMMARY . . . . .	1
INTRODUCTION . . . . .	2
Background Information . . . . .	2
TEST AND RESULTS . . . . .	5
Applicability to Apollo Vessels . . . . .	5
Analytical Procedure . . . . .	5
Specimen Preparation . . . . .	6
Analysis of Data . . . . .	6
Nondestructive Tests . . . . .	9
Apollo Pressure Vessel Analysis . . . . .	10
EVALUATION OF Ti-6Al-4V ALLOY PRESSURE VESSELS CONSIDERING EXPOSURE HISTORY PRIOR TO FLIGHT . . . . .	12
Vessel Analysis . . . . .	13
CONCLUDING REMARKS . . . . .	14
ADDENDUM, LUNAR MODULE VESSEL ANALYSIS . . . . .	15
REFERENCES . . . . .	22

## TABLES

Table		Page
I	APOLLO TITANIUM ALLOY PRESSURE VESSEL DATA . . . . .	17
II	Ti-6Al-4V FRACTURE TOUGHNESS AND TENSILE VALUES . . . . .	18
III	THRESHOLD VALUES FOR 6Al-4V TITANIUM ALLOY AND VARIOUS ENVIRONMENTS . . . . .	19
IV	CYCLIC FLAW GROWTH DATA IN VARIOUS ENVIRONMENTS . . . . .	20
V	ANALYSIS OF APOLLO BLOCK I TITANIUM PRESSURE VESSELS . . . . .	21

FRACTURE MECHANICS ANALYSIS OF APOLLO  
BLOCK I TITANIUM ALLOY PRESSURE VESSELS  
(COMMAND AND SERVICE MODULES)

By S. V. Glorioso and G. M. Ecord

SUMMARY

A fracture mechanics analysis of the titanium alloy pressure vessels on the Block I Apollo Command and Service Modules is presented. The proof pressure test is the base line for the evaluation of the pressure vessels with respect to maximum flaw size possible after proof testing. A subsequent linear elastic fracture mechanics analysis of the maximum possible flaws with respect to subcritical growth is made for the various Apollo pressure vessel environments.

The results show that in some cases, the maximum operating pressure of the vessels could cause flaw growth if the maximum flaw which would allow a successful proof test existed in the tank. In all cases, however, the normal operating pressure is below the pressure which would cause growth. The maximum pressure which will assure no flaw growth is specified for each vessel.

In the case of the Electrical Power System Cryogenic hydrogen vessel, it is shown that the present proof test (which is done at room temperature) will not screen out flaw sizes less than the vessel thickness, and, therefore, for the purpose of a fracture mechanics analysis, the proof test gives no usable information. The vessel design is controlled by the creep properties of the material at room temperature and consequently at the operating stress at cryogenic temperature the vessel is considered to be safe.

The rationale used in the analysis of the pressure vessels and related experimental data are included in this report.

## INTRODUCTION

The aerospace industry has always faced the serious problem of obtaining minimum weight spacecraft structures with maximum reliability. To minimize weight, high strength materials are being used under stress conditions associated with low safety factors. Unfortunately, the high strength conditions of many alloys presently in use for pressure vessels are sensitive to small flaws and various environments and, therefore, require advanced analytical and inspection techniques to insure reliability.

It is important to recognize that limitations in present nondestructive inspection techniques (which are subject to the vagaries of the inspector and depend on artificial reference flaws for interpretation) will allow flaws to escape detection. Attention must be given to the way in which these flaws may grow or propagate during ground testing and flight to insure that they do not result in failure of the pressure vessels during use.

This report presents a fracture mechanics analysis of the Apollo Command and Service Module (CSM) pressure vessels made of titanium alloys and an examination of inspection methods.

If properly designed, the proof test can be a valuable inspection tool although, in some cases, engineering limitations may prevent the test from being used to screen flaws as small as required to preclude a service failure.

The concepts of linear elastic fracture mechanics are used in this paper to examine the relationship of the maximum flaw size in a pressure vessel passing a proof test and the subsequent subcritical crack growth possible in ground test and flight environments. A fracture mechanics analysis based on a proof test of a pressure vessel considers only those flaws which may exist in the vessel after the proof test and their subsequent effect on the vessels under the known service requirements. The analysis does not incorporate effects on service life due to materials discrepancies or physical damage to the vessels subsequent to the proof test such as might be caused by improper handling or the use of fluids which are not considered in the analysis.

Background Information.- The fracture mechanics approach to the fracture toughness of a material has grown from a concept presented by Griffith (1) in 1920. Griffith postulated that the fracture strength of a very brittle material such as glass was governed by the behavior of the severest crack of a distribution of cracks in the material. He further suggested that the strength of the material could be calculated from solid state surface energy and crack size by a critical instability

relation. Instability was assumed to occur when the strain energy release rate with crack extension exceeded the rate of increase of surface energy.

Griffith's energy concept has been re-examined and modified by several investigators so that it could be applied to metals which are not so brittle as glass. In 1952, Irwin and Kies (2) showed that a modified form of the Griffith concept, in which plastic strain work is considered, could be employed in fracture strength analysis in the presence of substantial amounts of plastic strain so long as fracture occurred prior to general yielding. Irwin published data in 1957 (3) from which it was concluded that the energy release rate could be directly related to a parameter which has been designated the stress intensity factor,  $K$ .

In 1963 it was shown by Paris and Erdogan (4) that cyclic crack growth could also be related to the stress intensity factor. Subsequently, in 1965, it was demonstrated by Johnson and Willner (5) that slow corrosive crack growth also could be expressed as a function of the stress intensity factor.

The stress intensity factor approach to fracture toughness has been generally accepted as the best currently available means of utilizing fracture mechanics in practical problems. This is shown by the many publications appearing in the past few years and the general interest being expressed concerning the subject.

In the simplest terms, the fracture toughness parameter describes the maximum flaw that a material can tolerate without rapid fracture when loaded to a prescribed stress level. The fracture toughness parameter is the value obtained for the stress intensity factor which will result in flaw instability or material failure, and is denoted as the critical stress intensity factor,  $K_c$ . The minimum value of  $K_c$ , and hence the minimum value of stress for failure with a given flaw occurs when the state of deformation is plane strain. (Note: Plane strain is generally considered to exist when one of the three principal strains is zero or negligible). This minimum value of the fracture toughness parameter for a material is denoted as  $K_{IC}$ , and is described as the plane strain fracture toughness.

The stress intensity factor,  $K$ , is proportional to the product of the applied stress and the square root of the crack depth. Irwin (6) derived the expression relating the stress intensity factor, gross stress, and crack size for semi-elliptical surface flaws, and showed

that the state of deformation at any point on the flaw periphery was one of plane strain. Irwin's equation for stress intensity can be written

$$K_I = 1.1\sqrt{\pi} \sigma \left(\frac{a}{Q}\right)^{\frac{1}{2}} \quad (1)$$

where  $\sigma$  is gross stress and  $a/Q$  may be considered a normalized or "resolved" crack depth. The crack depth is "a," and "Q" is a parameter which primarily describes the shape of the crack. Q is dependent on the ratio of the crack depth, a, to the crack length, 2c. Q also depends, to a lesser extent, on the ratio of applied stress to the yield strength of the material. This results from the incorporation of a plasticity correction factor in calculated values for Q. The most severe crack is one which is long with respect to its depth. The value of Q for such a crack, if it is assumed to be elliptical, is approximately 1. Irwin's limits for the equation include the requirement that the crack depth, a, shall be less than one-half the thickness of the material and the gross stress,  $\sigma$ , shall be less than the yield stress of the material.

However, in order to analyze thin-walled pressure vessels (less than .125 inch thick for 6 Al-4V titanium alloy), it is necessary to know the stress intensity for flaws which are relatively deep with respect to vessel thickness. As the flaw depth increases to more than half the thickness of the material, the stress intensity as described by Irwin's equation must be magnified due to the effect of the free surface on the flaw tip. Tiffany, Masters and Pall (7) describe the use of appropriate magnification factors in conjunction with Irwin's equation. Values for the magnification factor obtained from reference (7) for flaws which are long with respect to depth (the most severe flaws) are presented in Figure 1 as a function of the ratio of flaw depth to material thickness, a/t.

The magnification factor,  $M_k$ , is applied to the Irwin equation to obtain the stress intensity for deep surface flaws. The resulting equation is written

$$K_I = 1.1\sqrt{\pi} \sigma \left(\frac{a}{Q}\right)^{\frac{1}{2}} M_k \quad (2)$$

## TESTS AND RESULTS

Applicability to Apollo Vessels.- Table I lists the pertinent information for the Apollo Command and Service Module (CSM) titanium alloy vessels which are analyzed in this report, including dome and cylindrical wall thicknesses, weld land thicknesses, and flight environments.

A primary consideration in evaluating each vessel is the assumed crack shape. In this report, it is assumed that flaws long with respect to their depths exist in the tanks ( $a/2c < .15$ ).  $Q$  may, therefore, be considered to be unity for this condition which represents the most severe flaw configuration.

Analytical Procedure.- The average fracture toughness and tensile properties obtained for Apollo titanium pressure vessel materials are presented in Table II. These data have been determined experimentally from test specimens representative of the pressure vessel material.

The value of the plane strain fracture toughness,  $K_{IC}$ , for the 6Al-4V solution-treated and aged (STA) titanium alloy forgings has been determined to be approximately  $44 \text{ ksi } \sqrt{\text{in.}}$  (8). That is, any combination of stress and crack size giving a stress intensity of  $44 \text{ ksi } \sqrt{\text{in.}}$  will, by equation 2, result in failure of the material. The crack size required to produce failure will vary with the thickness of the material. For example, a stress of 138 ksi in .053 in. thick material will cause failure if a crack .023 in. deep exists, while the same stress in .027 in. thick material will fail if a crack .017 in. deep exists. This difference in effective flaw size results from differences in the magnification factor,  $M_k$  in equation 2, which is dependent on the ratio of crack depth to wall thickness;  $M_k$  is 1.09 in the first case and 1.26 in the second case.

To investigate the compatibility of a pressure vessel material with the fluid it is intended to contain, stressed specimens with cracks were exposed to the fluid or environment in question. In the case of the 6Al-4V titanium alloy forgings, it was determined that for each environment tested an apparent threshold stress exists below which cracks in the alloy will not grow. For example, in the case of aerazine-50 this threshold value of stress intensity,  $K_{th}$ , is 80% of the critical stress intensity at 70° F (Figure 2). The threshold is chosen so that data from all specimens that failed or exhibited crack growth fall above the threshold. An analysis of pressure vessels using this threshold value would therefore be slightly conservative. This conservatism is desirable because, at the time, data from the large number of specimens necessary

for an adequate statistical analysis are not available. The experimental threshold values for other environments are listed in Table III.

Specimen Preparation.- Standard configuration tensile specimens (ASTM Specification E-8) are cut from vessel parent material and weldments. A shallow cut is made in the surface at midlength of the specimen by means of an electrical discharge machine (EDM). The specimen is then fatigued under tension-tension type loading to grow a flaw which propagates from the root of the EDM cut. This results in a polished, shiny crack easily discerned by fractographic examination after the specimen is tested. For determination of a static  $K_{IC}$  value, the fatigue-cracked specimen is loaded to failure in tension. The maximum gross stress (based on original cross-section area) and the exact dimensions of the fatigue crack, measured after the test, are used in equation 2 to calculate the fracture toughness ( $K_{IC}$ ) of the material. Should a constant-stress, flaw-growth test be desired, the specimen is loaded to a prescribed gross stress in the selected environment after the fatigue crack is generated. If failure does not occur in a predetermined time, the specimen is "fatigue marked." That is, it is again cycled in tension-tension loading to add a second polished portion to the crack area. The specimen is then tested to failure in tension. An area between the two fatigue-cracked zones indicates growth during the constant stress loading. A photographic example of a specimen showing the EDM cut, the initial fatigue crack, growth under constant stress in methanol and the final "fatigue mark" is shown in figure 3. The  $K_{IC}$  value for this specimen was determined from the measured stress necessary to break the specimen during the tensile test and the total flaw size which includes the fatigue mark. This value of  $K_{IC}$  was divided into the stress intensity value to which the specimen was loaded at the start of the fluid exposure,  $K_{Ii}$ , as determined from the constant stress and the initial fatigue crack size, to give the stress intensity ratio,  $K_{Ii}/K_{IC}$ .

Fatigue data reflecting cyclic flaw growth of precracked specimens determined in various environments are presented in Table IV.

Analysis of Data.- The application of the data from the static fracture toughness,  $K_{IC}$ , and the sub-critical flaw growth to a pressure vessel may be summarized as follows. The stress intensity ratio (the ratio of the initial stress intensity to the critical stress intensity,  $K_{Ii}/K_{IC}$ ) as a function of the time to failure for cracked specimens is obtained experimentally and gives a curve as shown in Figure 4(A).

The stress intensity ratio corresponding to the horizontal portion of the curve is the apparent threshold value for onset of flaw growth in the test environment. An increase of the stress intensity above this value will result in flaw growth. The flaw will continue to grow to the critical size at which rapid crack growth and failure occurs. Below the threshold value, observable growth does not occur.

A graph consisting of the threshold stress intensity and the critical stress intensity curves is constructed as illustrated in Figure 4(B). If a proof test is conducted at a stress  $\sigma_A$ , and failure does not occur, it can be assumed that no equivalent flaw equal to, or greater than,  $a_A$  exists at the end of the proof test. This information can be used to conclude that, if the pressure vessel is used at a stress level less than  $\sigma_B$  in the same environment, then crack growth will not take place during the constant stress operational life. A pressure vessel for this fluid should be designed such that the maximum operating stress gives a stress intensity below the threshold value.

It must be noted here that the data used in this report have been developed for relatively short time exposures. For missions longer than those of the current Apollo program, long time data must be obtained.

By use of this method of analyzing pressure vessels, it can be shown that safe operation can be predicted from the ratio of the proof pressure to the operating pressure, and from the threshold stress intensity ratio required for crack growth. The derivation follows:

$$\left(\frac{a}{Q}\right)_p = \text{flaw size screened by proof cycle}$$

$$\left(\frac{a}{Q}\right)_o = \text{maximum flaw size which will not grow at the operating pressure}$$

$$\sigma_p = \text{proof stress}$$

$$\sigma_o = \text{operating stress}$$

$$\gamma = \text{ratio of proof to operating stress, } \sigma_p/\sigma_o$$

$$R = \text{threshold stress intensity ratio } (K_{th}/K_{IC})$$

If  $\left(\frac{a}{Q}\right)_p \leq \left(\frac{a}{Q}\right)_o$  then no flaw exists in the vessel at the time of the proof test which could grow during the mission. Assuming  $\left(\frac{a}{Q}\right)_p = \left(\frac{a}{Q}\right)_o$  then the same magnification factor,  $M_k$ , applies to both cases.

$$K_{IC} = 1.1\sqrt{\pi} \sigma_p \left(\frac{a}{Q}\right)_p^{\frac{1}{2}} M_k \quad (3)$$

$$K_{th} = RK_{IC} = 1.1\sqrt{\pi} \sigma_o \left(\frac{a}{Q}\right)_o^{\frac{1}{2}} M_k \quad (4)$$

Dividing equation 3 by equation 4 and substituting  $\frac{\sigma_p}{rR}$  for  $\sigma_o$  gives

$$\frac{1}{rR} = 1 \text{ or if } \left(\frac{a}{Q}\right)_p < \left(\frac{a}{Q}\right)_o \text{ then } \frac{1}{rR} < 1$$

Therefore to guarantee no flaw growth  $\frac{1}{rR} \leq 1$ . In many Apollo vessels the ratio of proof to maximum operating stress is 1.33, so  $\frac{1}{1.33R} \leq 1$  and therefore  $\frac{K_{TH}}{K_{IC}}$  for the fluid environment in these vessels must be .75 or greater to assure safety at the maximum operating stress.

In this analysis the value of the fracture toughness of the material cancels out. A forging with a lower toughness than the average  $K_{IC} = 44 \text{ ksi}\sqrt{\text{in.}}$ , for example  $K_{IC} = 38 \text{ ksi}\sqrt{\text{in.}}$ , would allow a smaller flaw to be screened in the proof test than a forging with a higher toughness, such as  $K_{IC} = 49 \text{ ksi}\sqrt{\text{in.}}$ , however, the less tough forging would fail in service with a proportionally smaller flaw than the tougher forging. Therefore, any scatter in the static fracture toughness for the Apollo pressure vessels does not affect the analysis.

Nondestructive Tests.- The nondestructive test (NDT) methods which are presently being utilized on Apollo vessels are X-ray inspection of all welds and penetrant inspection of some tank surfaces. Inspection by X-ray can reveal both surface and subsurface flaws, whereas penetrant inspection can detect only those flaws which are open to the surface. Both inspection methods are dependent upon the technique and the training of the inspector. Therefore, the minimum flaw size which may be detected varies. For this reason a precise limit cannot be assigned to the size of flaw that will be detected by either inspection method. A few relatively large flaws have accidentally escaped detection in Apollo vessels in the past: one of the most recent examples was a .060 in. deep flaw in a LM descent gaseous oxygen tank which caused failure (10).

The ability of the human eye to resolve fine detail depends on the contrast between the detail and the surrounding medium. In penetrant inspection, excellent contrast is usually obtained between the flaw and the surrounding medium. A practical lower limit of flaw resolution in penetrant inspection is in the range from 0.001 to 0.0001 in.

In X-ray inspection, the lower limit of flaw detection is determined by the resolution capability of the equipment, and two percent sensitivity is considered excellent flaw resolution. For example, with a metal thickness of 0.050 in., resolution of 0.001 in. flaw would be considered excellent. However, most flaws in welds do not have sharply defined boundaries, and a more realistic limit of detection would be flaws having a least dimension three-or-four-times larger than the optimum limit (0.004 in. flaws in 0.050 in. thick material).

Because flaws caused by stress corrosion or fatigue cracking can be tightly closed, they are sometimes beyond the limits of detection by either inspection method, unless the inspection is performed under pressure to open the cracks.

In the case of metallurgical flaws in the material, such as massive embrittled alpha in titanium which may be caused by gas contamination during the melting process, no satisfactory method of detection is known. Such flaws are extremely rare but have caused failure in structures. Most notable is the failure during proof of a LM propellant tank (11).

In general, NDT techniques cannot be relied upon to guarantee flawless pressure vessels. NDT may save a vessel which would not survive a proof test; however, it is the proof test which provides the most dependable base-line for assurance of subsequent vessel performance.

Apollo Pressure Vessel Analysis.- Curves for each Block I titanium alloy pressure vessel are constructed showing the variation of flaw size with membrane stress and vessel pressure for the applicable stress intensities (critical and threshold). Because this flaw size varies with membrane thickness, curves are included for welds, hemispherical ends and the cylindrical portion of the vessels. Curves for the Block I SPS fuel and oxidizer tanks are included in Figures 5 through 10. The RCS fuel and oxidizer tanks are analyzed in Figures 11 through 14. The SPS helium vessel data are presented in Figures 15 and 16; and the CSM RCS helium vessel data are presented in Figure 17.

The data from Figures 5 through 17 are tabulated in Table V. The apparent maximum safe operation pressures and temperatures as determined by the fracture mechanics analysis are presented in column five of the table. These values represent those limits below which vessels which have survived the prescribed proof pressure will not experience flaw growth in the given environment. Safe operation of the pressure vessels is assured within these limits. Safe operation above these limits cannot be predicted because it is not known that all existing flaws are sufficiently small to preclude flaw growth and subsequent vessel failure. It is shown that pressures of SPS and RCS vessels containing  $N_2O_4$  at temperatures approaching  $105^\circ F$  must be held below the maximum operating pressure of the system to be assured safe.

In some cases vessel leakage will result before a flaw can grow to a critical size at operating pressures. An example of such a condition is illustrated in Figure 10. The longitudinal proof stress (axial) in the SPS oxidizer vessel weld area is shown to screen flaws .065 inch or larger. It can be seen that operation at normal or maximum system pressures would result in vessel leakage before a flaw oriented normal to the vessel axis (parallel to the weld) could grow to critical size. An analysis can also be made for the weld area of the SPS fuel vessels showing that under similar conditions leakage will occur. An examination of Figure 12 shows that the RCS oxidizer vessels will leak rather than rupture catastrophically while in operation below the apparent safe pressure limit.

For the fracture mechanics analysis of the vessels containing helium a threshold of  $.9 K_{IC}$  is assumed for gaseous helium. This value was chosen since it is believed that gaseous helium would have a threshold no lower than that of air which is  $.9 K_{IC}$ . The Command and Service Module helium vessels are analyzed simultaneously in Figure 15 since they are of the same dimensions and operate at the same design pressures.

The vessel welds are not analyzed graphically. Assuming the threshold  $K$  for gaseous helium in the weld area to be  $.9 K_{IC}$ , the maximum safe operating limit in the welds, expressed in vessel pressure, will equal that in the parent material. This is a reflection of the cancelling out of magnification factors in the formula for  $K_{IC}$  and  $K$  values as discussed in the Applicability section of this paper.

Figure 18 shows the analysis of the 5Al-2.5 Sn-titanium Extra-Low-Interstitials (ELI) grade cryogenic hydrogen vessel. The proof test provides no usable information, because the vessel thickness is less than the depth of flaw that is screened at the proof pressure of 400 psi. For the liquid hydrogen vessel, a cyclic analysis was made giving cycles to failure at the maximum operating pressure and  $-423^{\circ}$  F for various initial flaw depths as illustrated in Figure 19. Cyclic analyses were not made for the 6Al-4V titanium solution-treated and aged (STA) vessels because statistical cyclic data for this material are not available. The 6Al-4V titanium STA material was spot-checked using a minimum of fatigue specimens. The proof test screens out relatively small flaws in these vessels. Therefore, if the vessel life includes a minimum number of cycles the vessel will not be fatigue critical at normal operating pressures. However, it is desirable to hold cycling to a minimum since cyclic loading will grow any existing flaws. The growth is insignificant for each cycle but is additive.

The data utilized in the analysis of the liquid hydrogen vessel (Figure 18) are obtained from reference (9). The toughness at  $75^{\circ}$  F for 5Al-2.5 Sn-titanium ELI alloy is approximately  $116 \text{ ksi } \sqrt{\text{in.}}$  as compared to  $44 \text{ ksi } \sqrt{\text{in.}}$  for the 6Al-4V - titanium alloy in the solution-treated and aged condition. The  $K_{IC}$  data is plotted as stress versus flaw size together with the  $K_{IC}$  ( $44 \text{ ksi in.}$ ) value at  $-423^{\circ}$  F, since this gives the depth of crack at a given stress for failure at the operational temperature. The apparent threshold for subcritical growth in liquid hydrogen is 90 percent of  $K_{IC}$ , i.e. 90 percent of  $44 \text{ ksi } \sqrt{\text{in.}}$

The safety factor for this vessel is high because of the low temperature creep problem associated with this alloy (12), and the operational pressure is below the threshold for growth provided the vessel does not leak at the start of the mission. (A crack depth greater than the vessel thickness is required for growth at the maximum relief valve pressure of 300 psig.)

Since there is no way to determine the maximum flaw which could exist at the time of flight, various flaw depths were assumed in the

vessel varying from .005 inch deep to a depth equal to the vessel thickness. The number of fatigue cycles necessary to cause leakage at the maximum relief valve pressure and at liquid hydrogen temperature has been calculated from stress intensity ratio ( $K_i/K_{IC}$ ) vs cycles to failure data. This data is shown graphically in Figure 19. For example, a flaw .005 in. deep and wide with respect to its depth ( $Q = 1$ ) would require approximately 2400 cycles of stressing from 0 to 46.9 ksi, (0 to 300 psig tank pressure) to propagate to a depth equal to the vessel thickness. It can also be seen from the curve that if a flaw .005 in. deep was cycled 1000 times at 46.9 ksi, the flaw would have grown to a depth of about .012 inch. (It requires approximately 1400 cycles for a flaw .012 inch to grow to leakage.) In a similar manner, the number of cycles for any initial flaw depth to grow to a preselected flaw depth can be read from the curve.

Because cycling causes even the smallest flaw to grow, the number of cycles to which the vessels are subjected should be kept to a minimum.

#### EVALUATION OF Ti-6Al-4V ALLOY PRESSURE VESSELS CONSIDERING EXPOSURE HISTORY PRIOR TO FLIGHT

The preceding analysis of Apollo titanium alloy vessels does not consider interim exposures to various fluids and pressures after proof testing and prior to flight. Figures 20 and 21 are graphic illustrations of  $K_{IC}$  values for Ti-6Al-4V alloy forgings and welds with threshold K values of some of the fluids which have been used in Apollo vessels under pressure. The data presented in these figures correspond to SPS oxidizer tank cylinders which were analyzed in Figure 8 and SPS oxidizer vessel welds which were analyzed in Figure 10.

Reference to Figure 20 shows that a vessel proofed at a stress of 138 ksi may experience flaw growth if exposed to Freon MF at stresses above approximately 75 ksi. In the case of the SPS oxidizer vessel, this stress corresponds to a pressure slightly above the normal operating pressure of 175 psi. Flaw growth at this stress could occur only if the largest possible flaw after proof testing at 138 ksi existed in the vessel. Smaller flaws would require correspondingly higher stresses for growth.

In addition to the threshold values shown in Table III preliminary experimental data indicate that Freon TF, another fluid used in some Apollo titanium pressure vessels, has a threshold K value comparable to that of aerazine-50.

The pressure-fluid history of any Apollo Ti-6Al-4V alloy pressure vessel from initial proof to flight can be examined for indications of pressure-fluid combinations which may have resulted in tank degradation by use of data such as presented in Figures 20 and 21. If there is an indication that tank degradation has occurred, the individual vessel must be examined in detail to determine its reliability. As an example, such an analysis has been made for the SPS oxidizer and fuel vessels on Apollo spacecraft 012.

Vessel analysis.- The SC012 SPS oxidizer vessels were originally proof tested at 325 psi. This verified that flaws greater than  $\left(\frac{a}{Q}\right)$  of .03 in. did not exist in the weld heat-affected zones (refer to Figure 21). Subsequent to the proof test the vessels were exposed to helium, nitrogen, and Freon MF. As can be seen in Figures 20-21, in an air or helium environment there existed no flaw which could grow at a pressure of approximately 290 psi or less and in Freon MF at 75° F, no flaw existed which could grow at a pressure of approximately 122 psi, or less. However, these vessels were exposed to Freon MF under a pressure of 240 psi for 48 hours and 275 psi for 5 minutes. Reference to Figure 21 shows that a flaw as small as  $\left(\frac{a}{Q}\right)$  of .008 in. could have grown. The proof test screened flaws only as small as  $(a/Q)$  of .030 in. It therefore is certain only that no flaw of  $\left(\frac{a}{Q}\right)$  approximately .038 in. or greater exists in the vessels (corresponding to the critical flaw size at 275 psi). For this reason, to be assured safe, exposure to inhibited nitrogen tetroxide must be held to a pressure below 215 psi at 70° F and below 190 psi at 105° F. These pressures apply to flaws aligned perpendicular or parallel to the girth weld even though the axial membrane stress is approximately one-half the hoop membrane stress. For flaws parallel to the girth weld, the 275 psi pressure would screen flaws no smaller than  $(a/Q)$  of .074 in. Should this flaw grow, the vessel would leak rather than fail catastrophically at the above suggested operating pressures.

A similar analysis of the cylindrical and dome sections of the vessels showed that the weld area, analyzed above, is the most critical consideration and is the governing factor in the safe pressurization of the oxidizer tanks.

The SC012 SPS fuel sump vessel was re-proofed at 300 psi. This indicates that flaws no larger than  $(a/Q)$  of .033 in. existed in the weld heat affected zones (Figure 7). The only environment to which the vessel has been exposed subsequent to this proof is gaseous helium at 240 psi. This is well below the threshold pressure for growth in helium for .033 in. flaws. (Calculation shows that a flaw approximately

.04 in. deep is required for growth in gaseous helium at 240 psi.) As can be determined in Figure 7, this vessel is assured safe as long as the pressure is maintained below approximately 230 psi at 110° F. This maximum is slightly below the system maximum operating pressure but well above the normal operating pressure.

#### CONCLUDING REMARKS

The fracture mechanics analyses of the titanium alloy pressure vessels on the Apollo Command, Service and Lunar Modules demonstrated the value of the proof test to determine the maximum possible initial flaw sizes in the various portions of the vessels. Nondestructive tests such as X-ray and penetrant inspection when used on a production basis, will not reliably detect all flaws that are large enough to cause problems by sub-critical growth when exposed to various environments. Since only one flaw is needed to cause failure, the assurance provided by the proof test is necessary in most cases.

Apollo Block I, CSM titanium vessels and Lunar Module vessels can be assured to be safe if the operating pressures are held to maximum values at the indicated temperatures as predicted by the analysis. Should the vessel be exposed after the initial proof test to fluids other than those considered in the analysis which could cause sub-critical flaw growth, then the initial proof does not assure safety and each tank must be analyzed on an individual basis.

The following recommendations are made:

- (1) The time at the proof pressure should be held to a minimum.
- (2) The number of pressure cycles should be kept to a minimum.
- (3) During the mission, the pressure and/or temperature should not be allowed to increase above the value that would cause flaw growth as predicted by the apparent threshold stress intensity and the maximum flaw screened by the proof test.

## ADDENDUM A

Fracture Mechanics Analysis of the Lunar  
Module Ascent and Descent Propellant Vessels

The Lunar Module (LM) propellant vessels have been analyzed in the same manner as the Command and Service Module pressure vessels. The fracture toughness and threshold values used for the Command and Service Module analysis are applicable to the LM vessels since the material of fabrication (Ti-6Al-4V forgings) and heat treat condition (Solution Treated and Aged) are the same. Figures 1A through 4A illustrate stress versus flaw size curves for the ascent and descent state pressure vessels. The fuel and oxidizer vessels in the ascent stage are identical in configuration and pressure requirements as are the fuel and oxidizer vessels in the descent stage. The respective curves, therefore, are applicable to both the fuel and the oxidizer pressure vessels.

Examination of Figures 1A and 2A shows that after a normal proof test the Lunar Module ascent vessels are assured safe at the normal operating pressure in any environment or at any temperature where the flaw growth threshold value for the pressurizing fluid is slightly greater than  $.60 K_{IC}$ . Reference to Table III shows that this assures safe operation for the fuel and the oxidizer vessels while at normal operating pressure. If the maximum operating pressure is encountered, the stress intensity for an assumed maximum permissible flaw is  $.75 K_{IC}$ , and in this case safe operation is assured only at temperatures below  $85^{\circ}\text{F}$  for the oxidizer vessels and  $110^{\circ}\text{F}$  for the fuel vessels.

Examination of Figures 3A and 4A shows that the Lunar Module descent vessels are assured safe at the normal operating pressure in any environment and at any temperature where the flaw growth threshold value for the pressurizing fluid is  $.70 K_{IC}$  or greater. Reference to Table III shows that this assures safe operation for the oxidizer vessels to  $105^{\circ}\text{F}$  and for the fuel vessels to at least  $110^{\circ}\text{F}$  while at normal operating pressure. Should maximum operating pressure be encountered the oxidizer vessels are assured safe at temperatures below  $90^{\circ}\text{F}$  and the fuel vessels at temperatures below  $110^{\circ}\text{F}$ .

It should be noted that the burst disc design for the descent propulsion system has a tolerance which could allow a vessel pressure as high as 308 psi. Operation at this pressure, assuming the existence of the maximum size flaw which could pass the proof test, would provide a stress intensity of  $.85 K_{IC}$  at the flaw tip. At this stress intensity flaw growth in fuel or oxidizer is highly probable.

Cyclic flaw growth of the ascent and descent propellant tanks does not appear to be a significant consideration during cyclic service to normal operating pressure. The proof test assures a cyclic life of approximately 120 cycles at the maximum operating pressure.

No matter what the past vessel history, the next proof cycle cannot be guaranteed against catastrophic failure by fracture mechanics analysis or other nondestructive techniques. Therefore, it is recommended that cycling to proof stresses should be kept to a minimum.

TABLE I.- APOLLO TITANIUM ALLOY PRESSURE VESSEL DATA

System (c)	Vessel	Environment	Vessel material	Minimum weld lend thickness, in.	Minimum dome thickness, in.	Minimum cylinder thickness, in.
SPS	Fuel Oxidizer	Aerozine-50 N <sub>2</sub> O <sub>4</sub>	Ti-6Al-4V STA <sup>a</sup>	0.070 .078	0.027 .030	0.053 .060
CM RCS	Oxidizer	N <sub>2</sub> O <sub>4</sub>	"	.065	.020	.020
SM RCS	Oxidizer	N <sub>2</sub> O <sub>4</sub>	"	.065	.017	.017
SPS	Helium	Gaseous helium	"	.750	.450	NA
CM RCS	Helium	Gaseous helium	"	-	.102	NA
SM RCS	Helium	Gaseous helium	"	-	.102	NA
SM/EPS	Hydrogen	Liquid hydrogen	Ti-5Al-2.5 Sn ELLI <sup>b</sup>	.083	.046	NA

<sup>a</sup>GTA - Solution treated and aged forging.

<sup>b</sup>ELI - Extra low interstitial.

(c) System: CM - command module, SM - service module, SPS - service propulsion system, RCS - reaction control system, EPS - electrical power system

TABLE II.- Ti-6Al-4V FRACTURE TOUGHNESS AND TENSILE VALUES

Material	Approx. spec. thickness	Avg. $K_{IC}$ , ksi $\sqrt{\text{in}}$	Range	Avg. ult. strength, ksi	Avg. yield strength, ksi
Lunar orbitor forging 'A'	0.125	<sup>a</sup> 43.6	42.9-44.2	165.8	156.9
Lunar orbitor forging 'B'	.125	<sup>a</sup> 45.3	38.8-48.1	169.1	157.1
Lunar orbitor forging 'C'	.125	<sup>a</sup> 45.6	42.9-48.7	160.3	159.4
Lunar orbitor forging 'C'	.02	<sup>a</sup> 43.5	39.2-47.7	--	--
Allison tank cylinder S/N 73 WCZ	.058	<sup>a</sup> 45.8	44.8-46.4	<sup>f</sup> 175.1	<sup>f</sup> 164.3
Allison tank weldment-HAZ <sup>c</sup>	<sup>d</sup> .045	<sup>a</sup> 39.3	36.9-44.2	132.7	126.4
Allison tank cylinder #1 <sup>e</sup>	.057	<sup>a</sup> 48.6	48.2-49.0	--	--
Allison tank cylinder #2 <sup>e</sup>	.057	<sup>a</sup> 41.5	39.9-43.0	--	--
Ti-5Al-2.5 Sn ELI <sup>b</sup>	.184	<sup>e</sup> 116 @ 75° F <sup>h</sup> 44 @ -423° F	--	--	--

<sup>a</sup>Data obtained from reference (8).

<sup>b</sup>Data obtained from reference (9).

<sup>c</sup>Material supplied by Allison Div. of General Motors for test purposes.

<sup>d</sup>Weldments milled to 0.045-inch thickness to remove misalignment in original weld.

<sup>e</sup>Cylinders from fuel tank which previously failed while exposed to methyl alcohol.

<sup>f</sup>Data obtained by Allison Div. of General Motors.

<sup>h</sup>116 ksi  $\sqrt{\text{in}}$  toughness for the Ti-5Al-2.5 Sn ELI alloy was a "pop in" value on a "through the thickness" type specimen.

TABLE III.- THRESHOLD VALUES FOR 6Al-4V TITANIUM ALLOY  
AND VARIOUS ENVIRONMENTS<sup>a</sup>

Environment	Temperature, °F	Threshold, $K_{th}/K_{IC}$	
		Parent metal	Weld HAZ <sup>b</sup>
Distilled water	65	0.86	0.86
Inhibited distilled water	72	.82	.82
Aerozine-50	70	.80	-
	110	.75	.75
Freon MF	65	.58	.40
Methanol	72	.24	.20
Nitrogen Tetroxide (NO = 0.25)	70	.80	.80
	105	.70	.70
Monomethylhydrazine (MMH)	105	.75	.75

<sup>a</sup>Data obtained from NASA Contract NAS 9-6665, The Investigation of Flaw Growth Characteristics of 6Al-4V Titanium, The Boeing Co., Seattle, Wash.

<sup>b</sup>Crack location 0.030 inch from weld - parent metal interface in heat-affected zone (HAZ).

TABLE IV.- CYCLIC FLAW GROWTH DATA IN VARIOUS ENVIRONMENTS<sup>a</sup>

Material	Temperature, °F	Environment	$K_{Ii}/K_{IC}$	Cycles to failure <sup>b</sup>
Lunar orbitor forgings	72	Aerozine-50	.614	1755
			.921	96
Allison weldment (HAZ)	105	Aerozine-50	.888	1044
			.922	516
Allison cylinder	65	Freon MF	.423	4116
			.582	595 171
	75	Distilled water	.518	1369
			.566	757
			.752	122
	75	Inhibited distilled water <sup>c</sup>	.542	1744
			.573	1054
			.712	338

<sup>a</sup>Data from reference 8.

<sup>b</sup>5 cpm, stress ratio 0.5

<sup>c</sup>500 ppm Sodium Chromate added to distilled water.

TABLE V.- ANALYSIS OF APOLLO BLOCK I TITANIUM PRESSURE VESSELS

Vessel	Fluid	System normal operating pressure, psi	System maximum operating pressure, psi	Maximum safe operating pressure <sup>a</sup>	
				psi	°F
SM/SPS - fuel	Aerozine-50	175	240	260 240	70 110
SM/SPS - oxidizer	N <sub>2</sub> O <sub>4</sub>	175	240	260 230	70 105
CM/RCS - oxidizer	N <sub>2</sub> O <sub>4</sub>	205	360	380 340	70 105
SM/RCS - oxidizer	N <sub>2</sub> O <sub>4</sub>	185	248	265 230	70 105
SM/SPS - helium	Helium	4050	4400	5250	80
CM and SM/RCS - helium	Helium	-----	5000	6000	80
SM/SPS - cryogenic hydrogen	Liquid hydrogen	230	300	NA	NA
CM/RCS - fuel	MMH	205	360	360	105
SM/RCS - fuel	MMH	185	248	248	105

<sup>a</sup> Pressures and temperatures below which safe operation is assured.

## REFERENCES

1. A. A. Griffith "The Phenomena of Rupture and Flow in Solids," Royal Soc. (London) Phil. Trans., Series A, Vol. 221 (1920) pp. 163-198.
2. G. R. Irwin and J. A. Kies, "Fracturing and Fracture Dynamics," Welding J. Res. Suppl., pp. 955 to 1005, (1952).
3. G. R. Irwin, "Analysis of Stresses and Strains Near the End of a Crack," J. of Applied Mechanics, Vol. 24, p. 361 (1957).
4. P. Paris and F. Erdogan, "A Critical Analysis of Crack Propagation Flaws," J. of Basic Engineering, Dec. 1963.
5. H. H. Johnson and A. M. Willner, "Moisture and Stable Growth in a High Strength Steel," Applied Materials Research, Jan. 1965.
6. Irwin, G. R., "Crack Extension Force for a Part-Through Crack in a Plate," J. of Applied Mechanics, Vol. 84E No. 4, Sec. 1962, pp. 651-654.
7. Tiffany, C. F.; Masters, J. N.; Pall, F.; "Some Fracture Consideration in the Design and Analysis of Spacecraft Pressure Vessels." Presented at ASM National Metals Congress, Chicago, Ill., Oct., 1966.
8. Contract NAS 9-6665 with the Boeing Airplane Company, Seattle, Wash., "Investigation of Flaw Growth Characteristics of 6Al-4V Titanium Alloy."
9. Tiffany, C. F.; Lorenz, P. M.; Hall, L. R.; "Investigation of Plane-strain Flaw Growth in Thick-walled Tanks," NASA CR-54837, Feb. 1966.
10. Unpublished Data, NASA Memorandum, "Electron Fractographic Analysis of Failed LM Descent Stage Gaseous Oxygen Pressure Vessel," ES4 to EC9, September 1966.
11. Allison Div. of General Motors Materials Laboratories Report No. 65-FA-8-6, April 1965.
12. Beech Aircraft Corporation, Test Report No. BR 13847, September 1963.

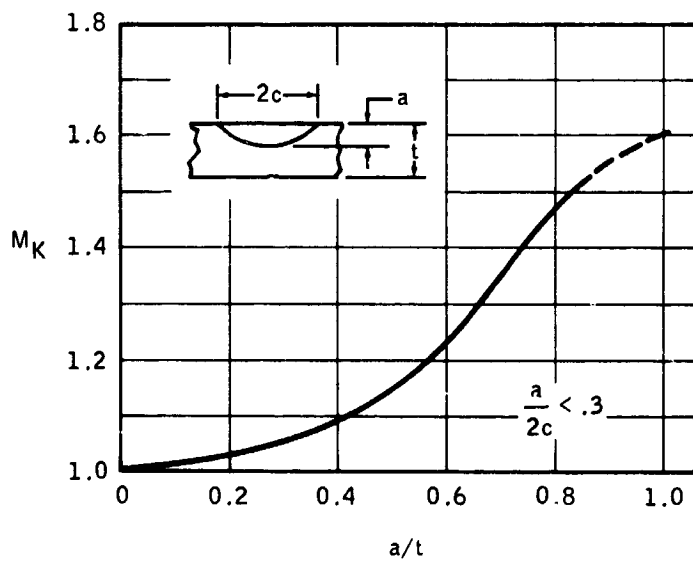


Figure 1. - Magnification factor for deep surface flaws.

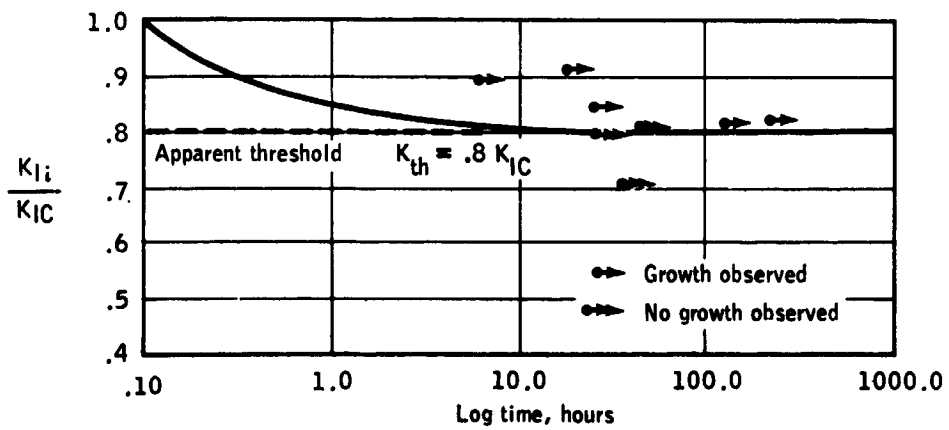
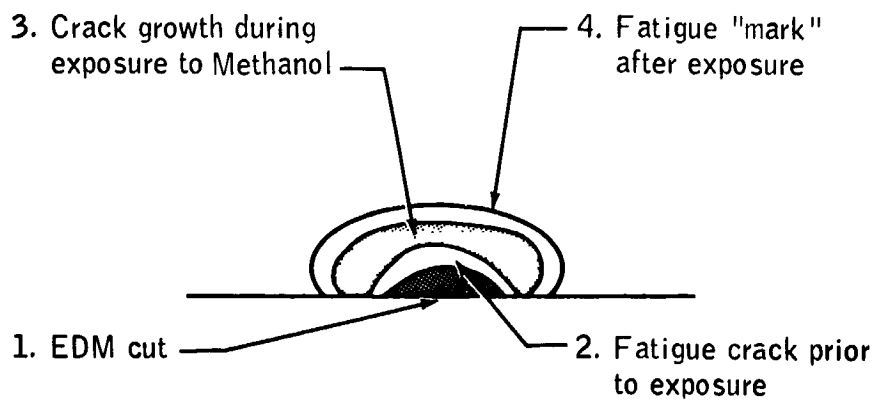


Figure 2. - Threshold determination from flaw growth data for 6Al-4V titanium alloy in aerozine 50 at 70°F.



(a) Fractograph of test specimen.



(b) Explanation of characteristics.

Figure 3. - Flaw characteristics for Ti-6Al-4V test specimens exposed to methanol.

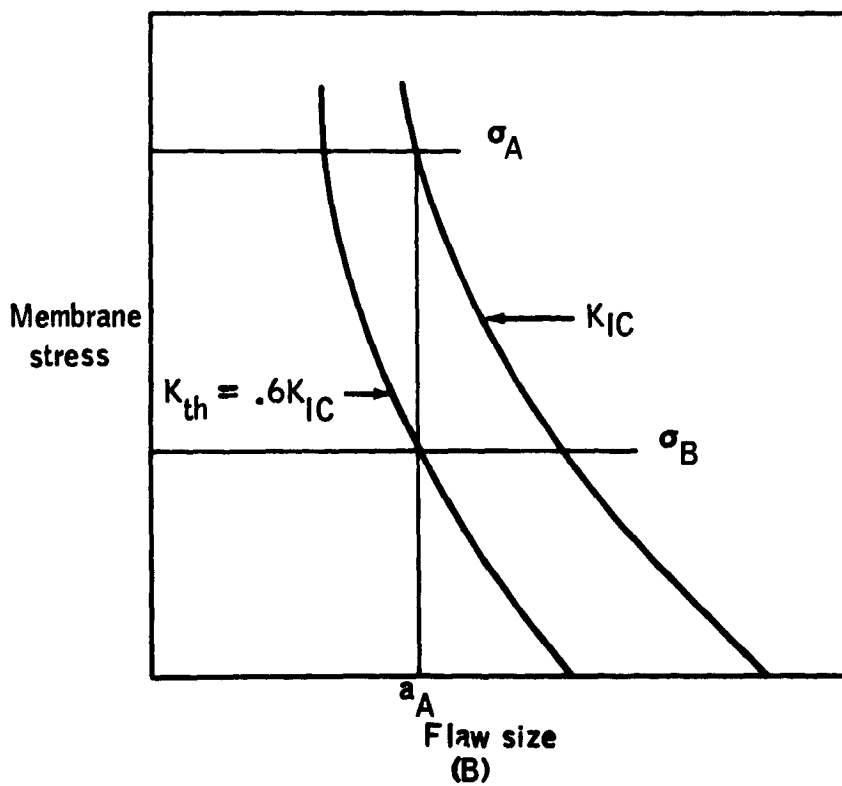
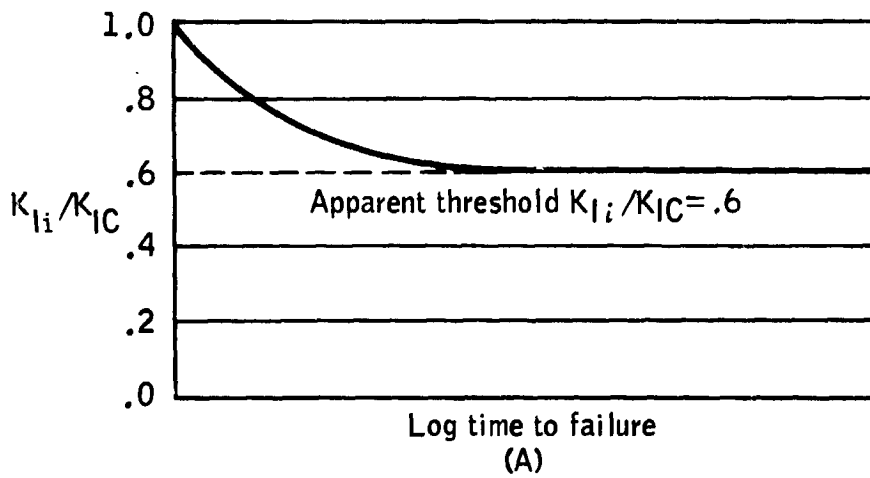


Figure 4. - Application of static fracture toughness and subcritical flaw growth to pressure vessel analysis.

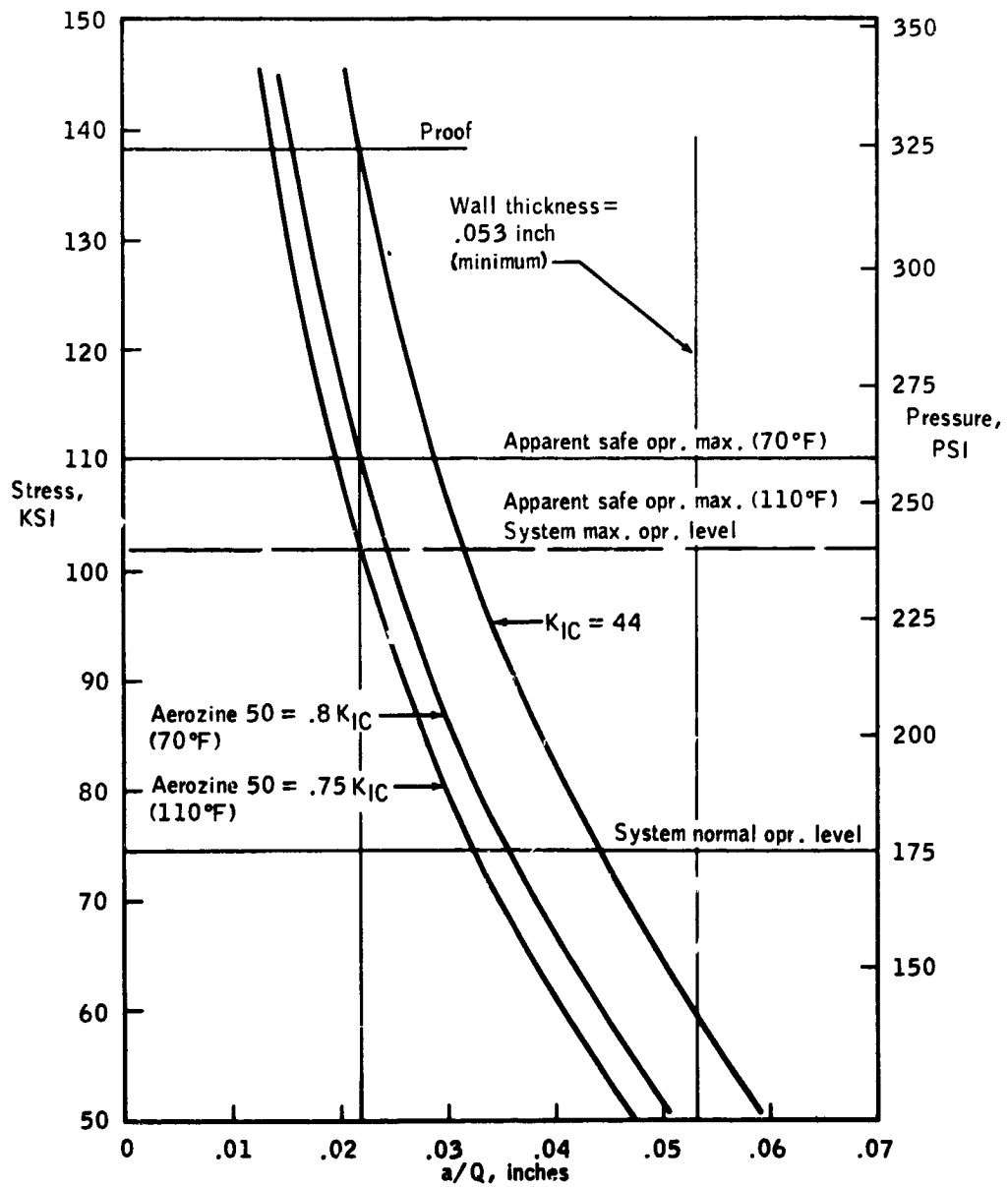


Figure 5. - Analysis of SPC fuel vessel cylinder proof test and operating conditions.

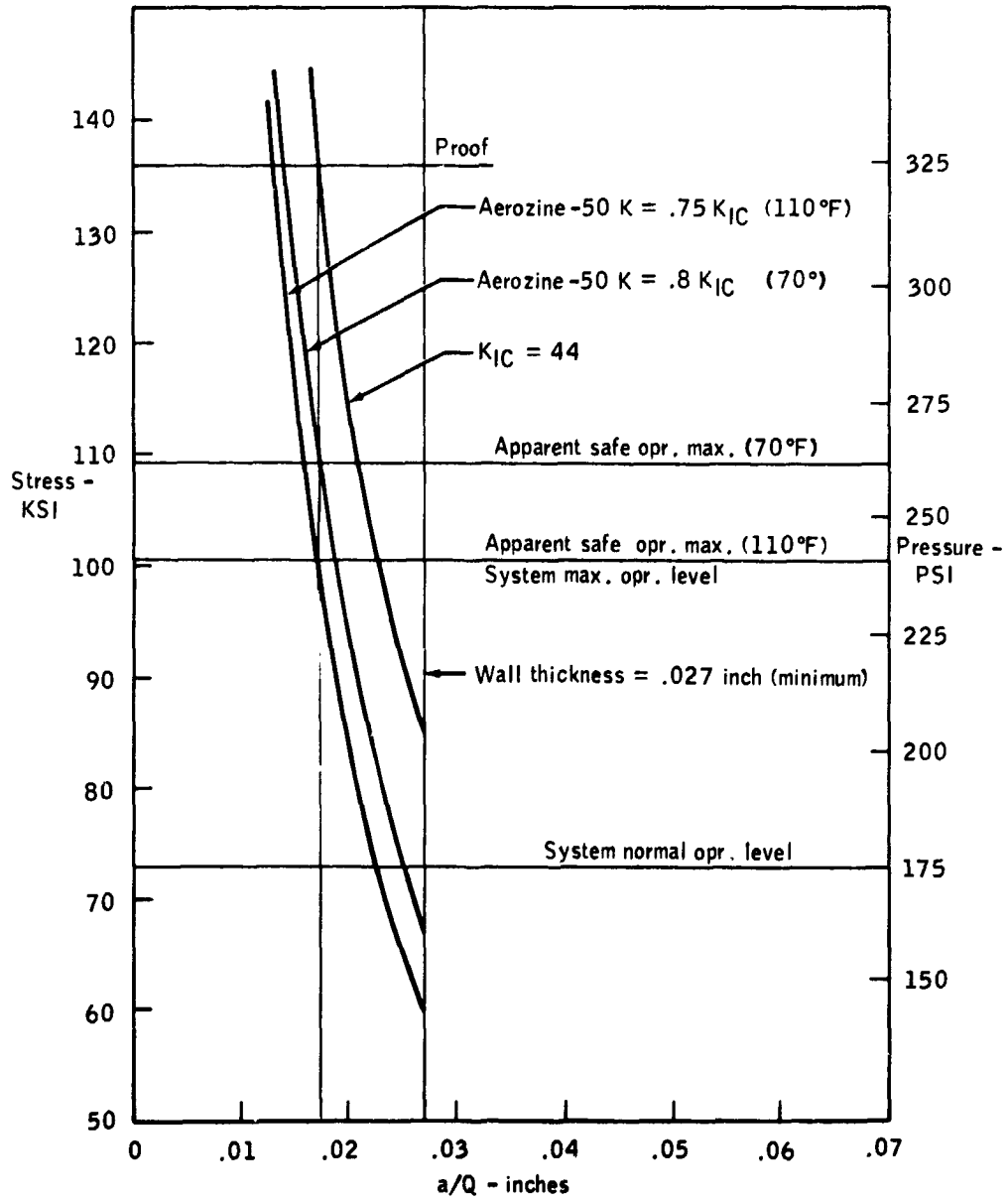


Figure 6. - Analysis of SPS fuel vessel dome proof test and operating conditions.

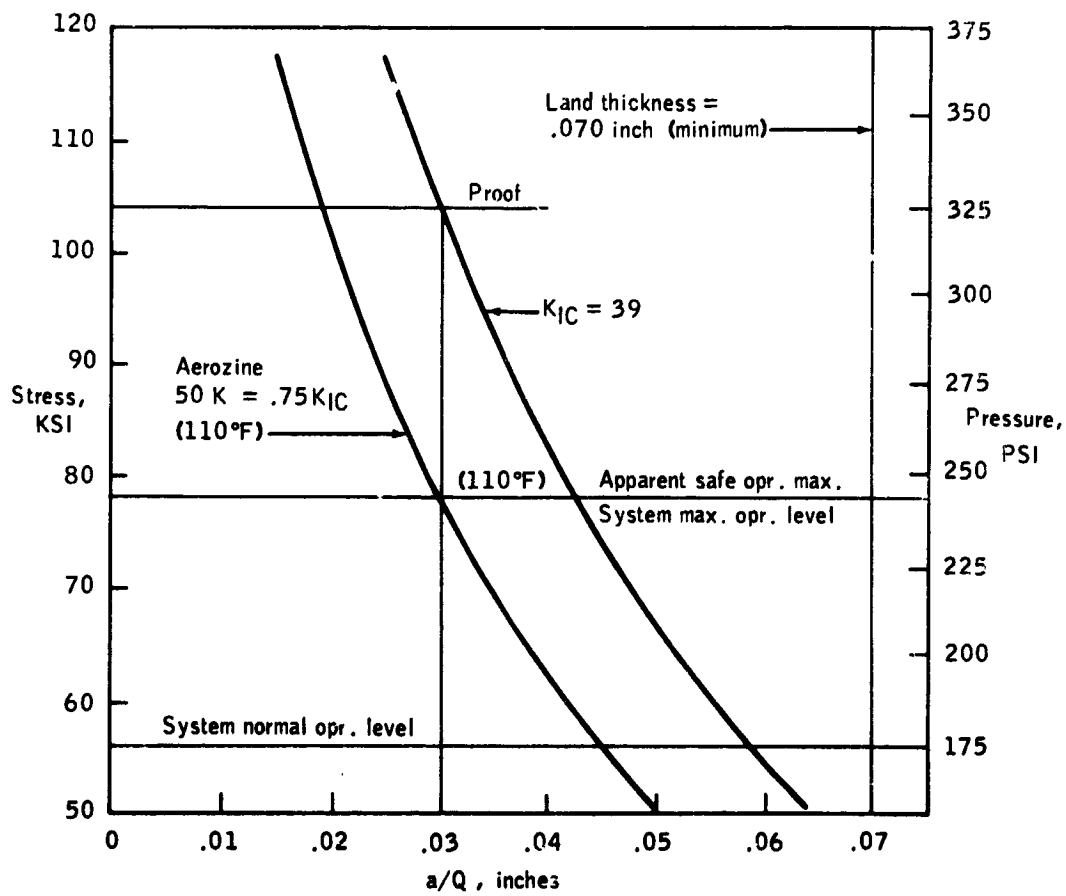


Figure 7. - Analysis of SPS fuel vessel weld zone proof test and operating conditions.

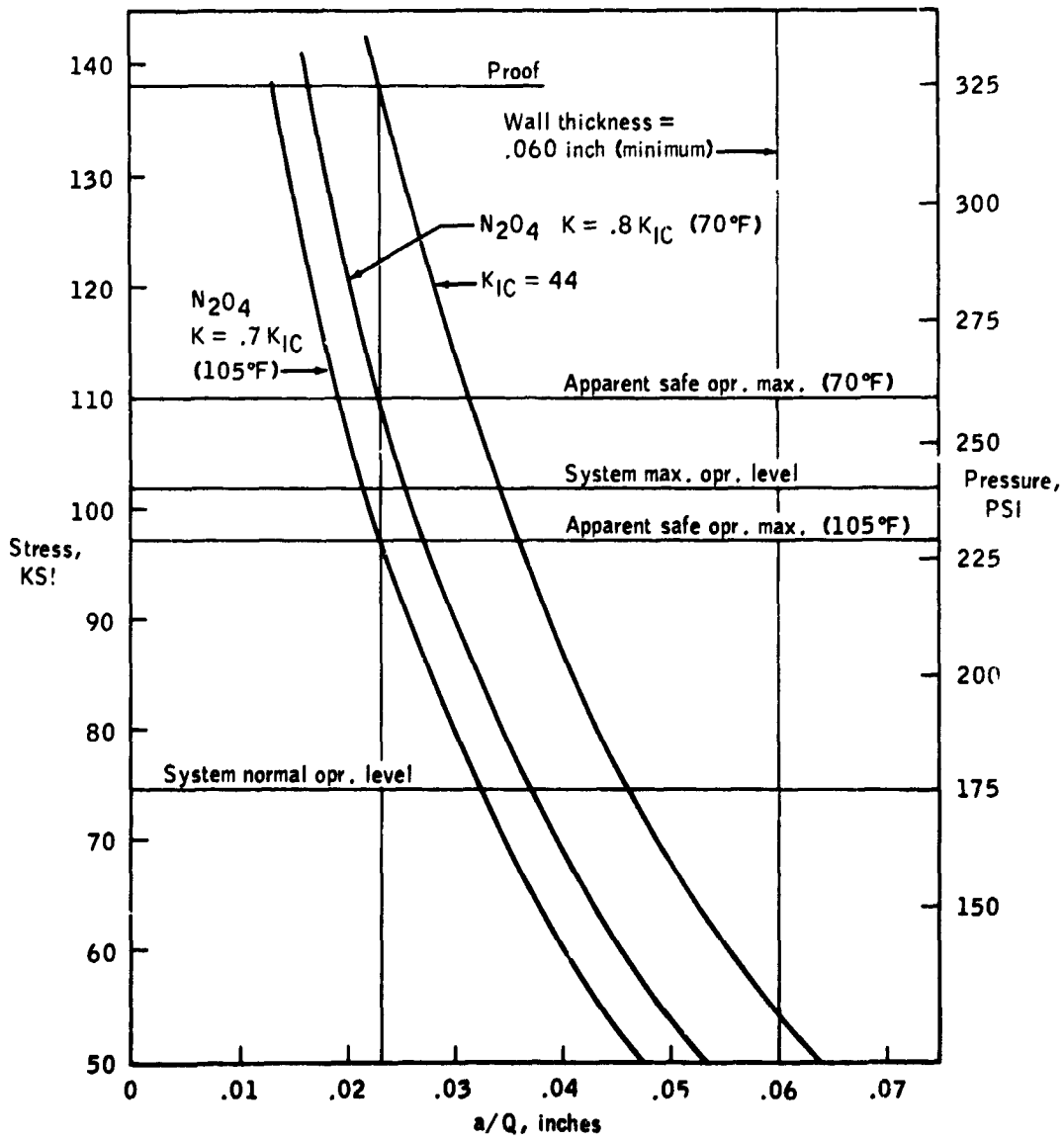


Figure 8. - Analysis of SPS oxidizer vessel cylinder proof test and operating conditions.

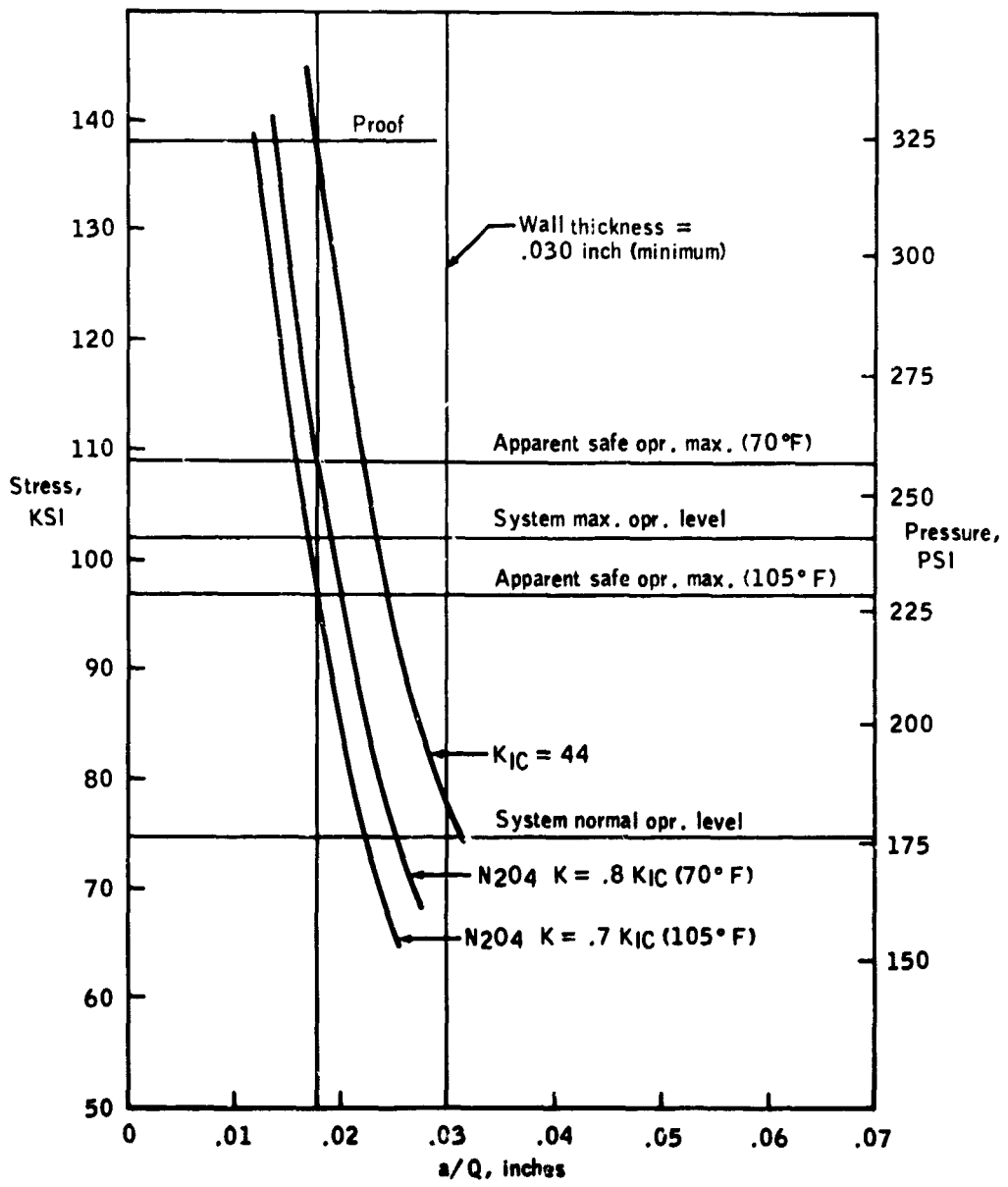


Figure 9. - Analysis of SPS oxidizer vessel dome proof test and operating conditions.

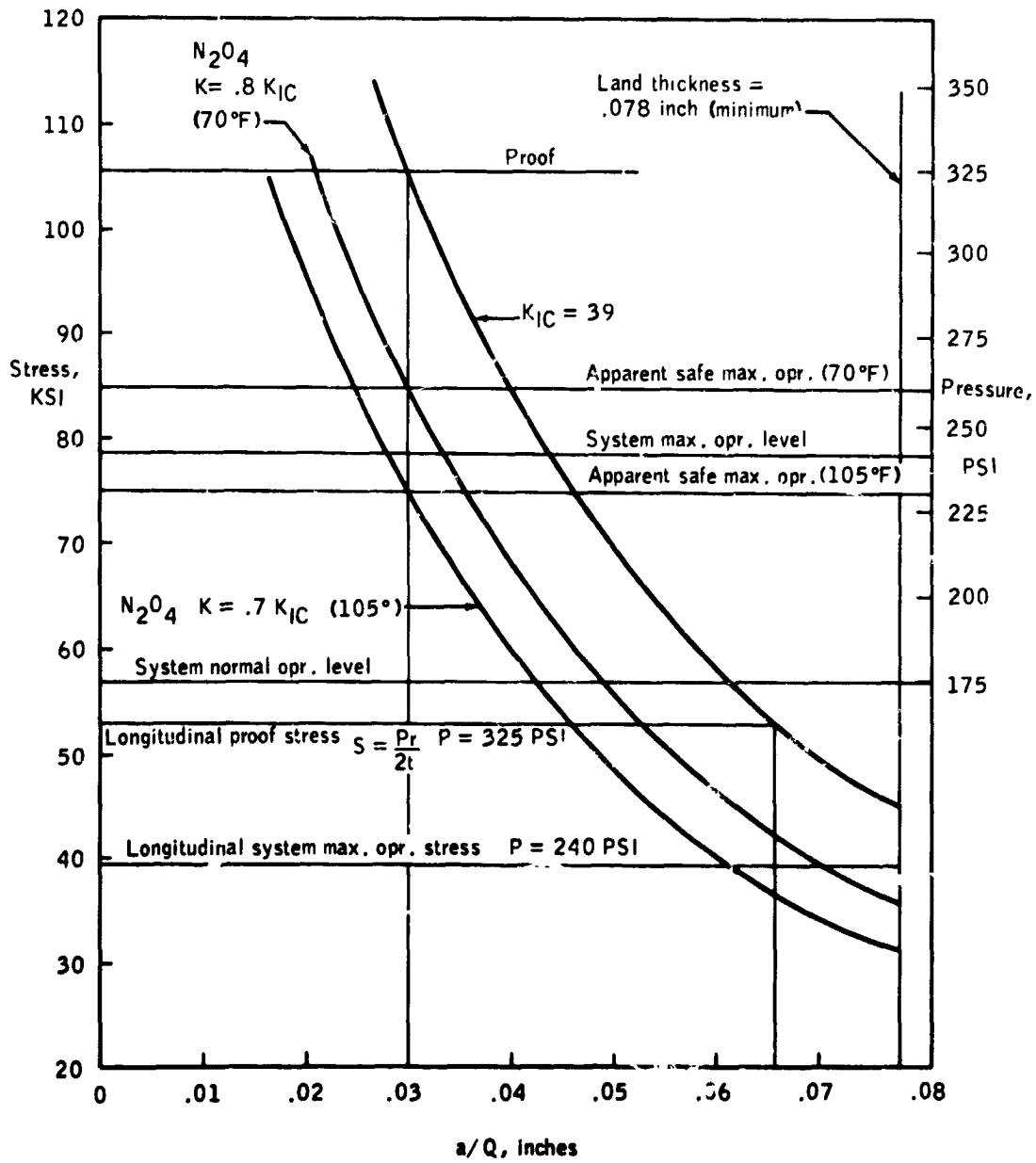


Figure 10. - Analysis of SPS oxidizer vessel weld zone proof test and operating conditions.

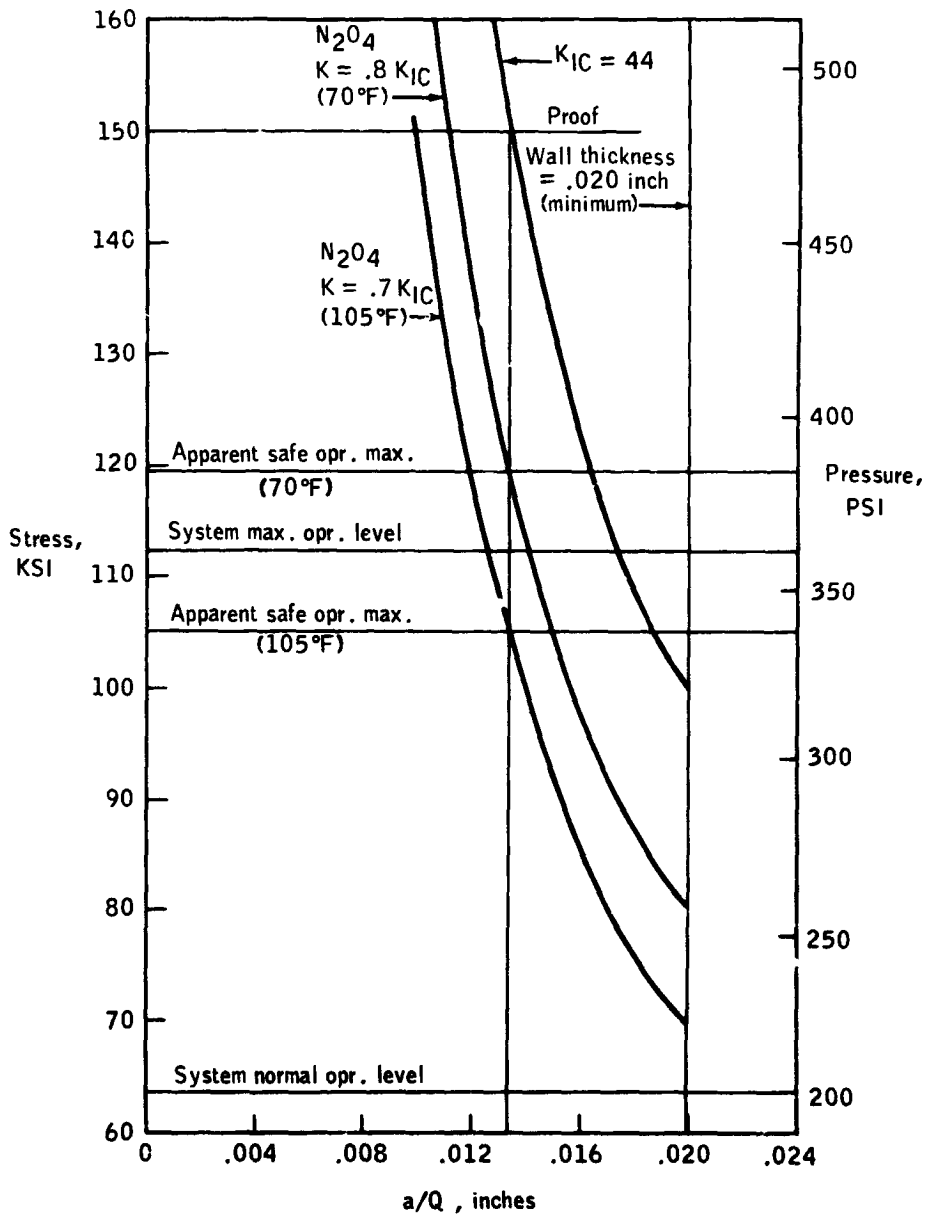


Figure 11. - Analysis of CM RCS oxidizer vessel proof test and operating conditions.

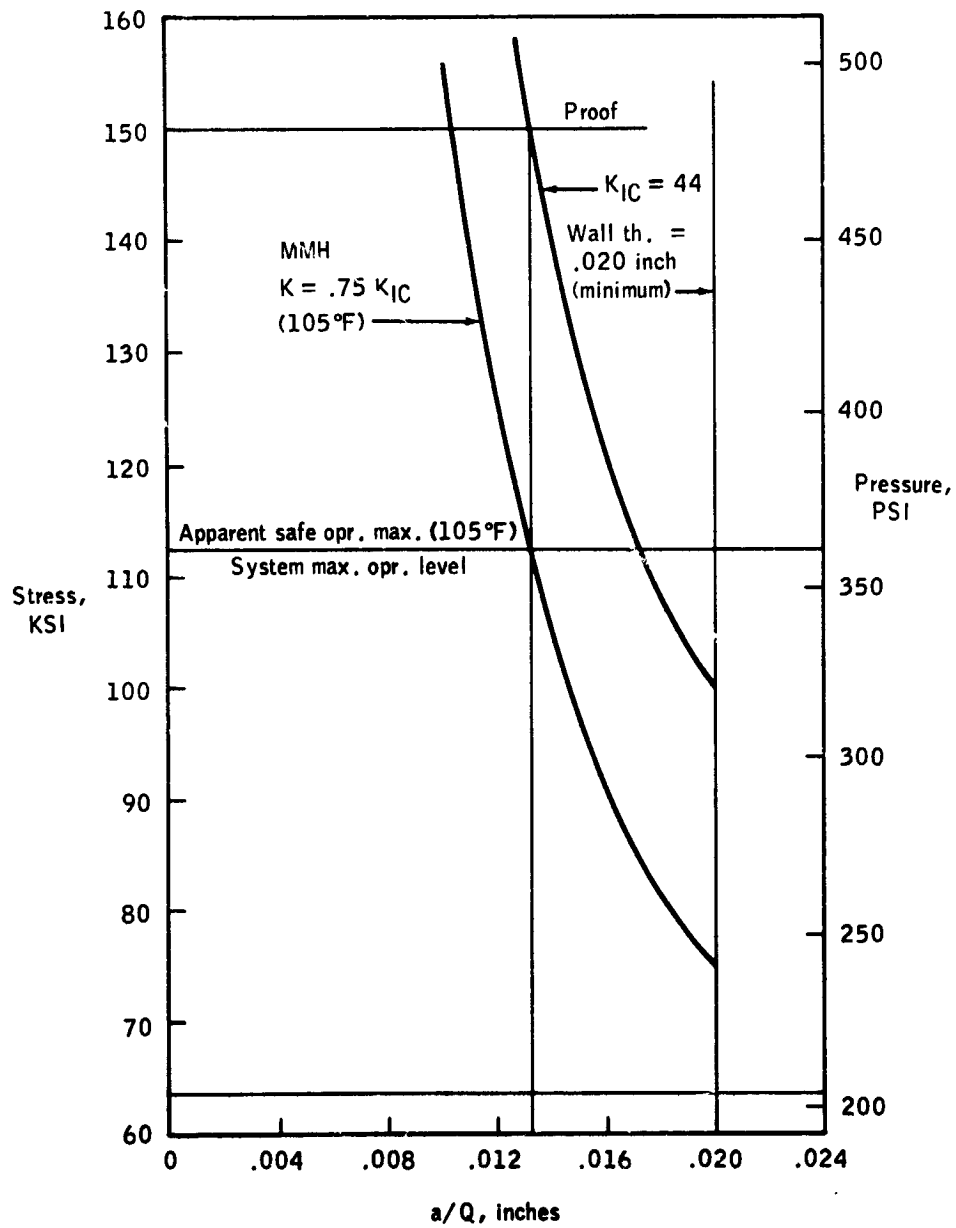


Figure 12. - Analysis of CM RCS fuel vessel proof test and operating conditions.

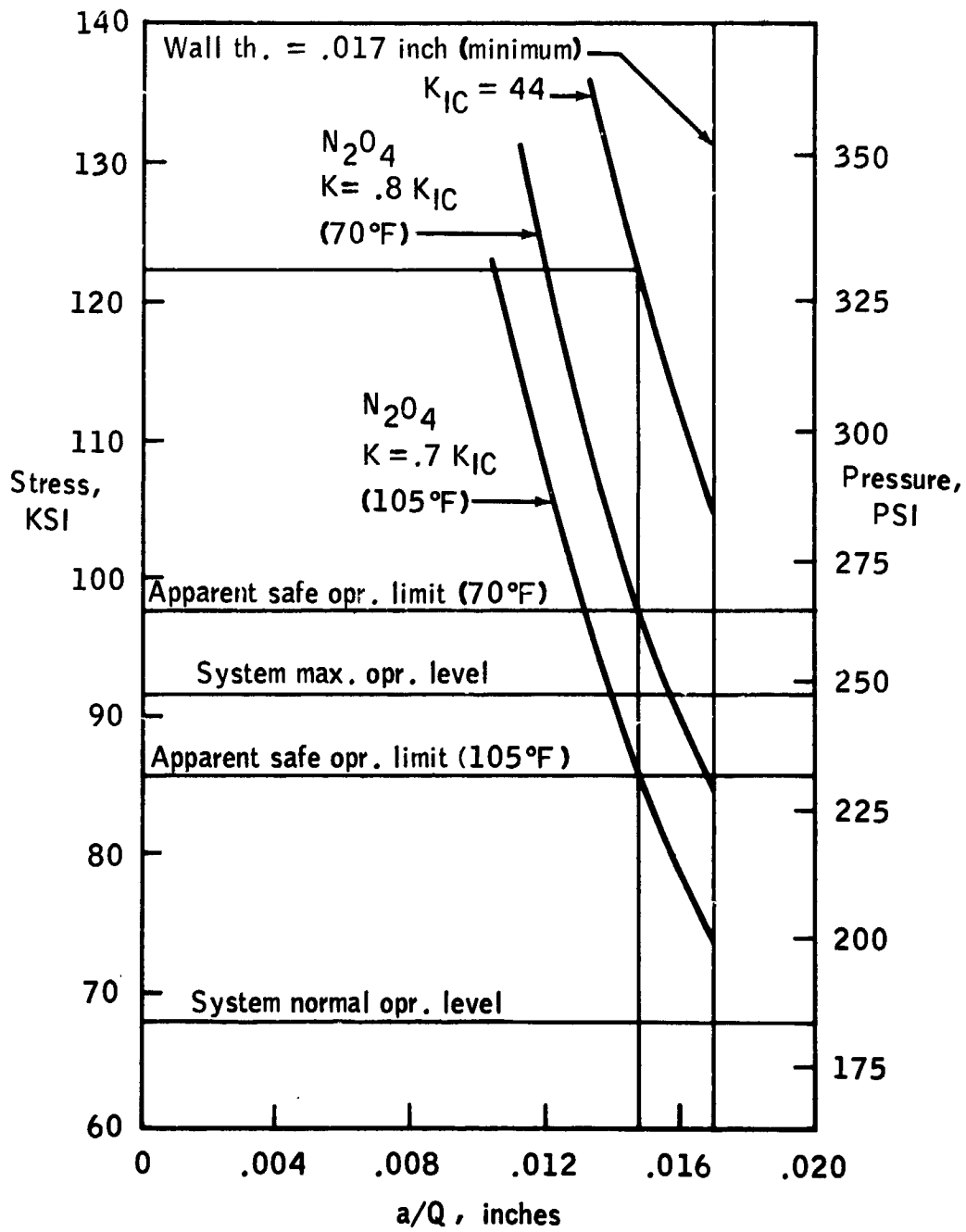


Figure 13. - Analysis of SM RCS oxidizer vessel proof test and operating conditions.

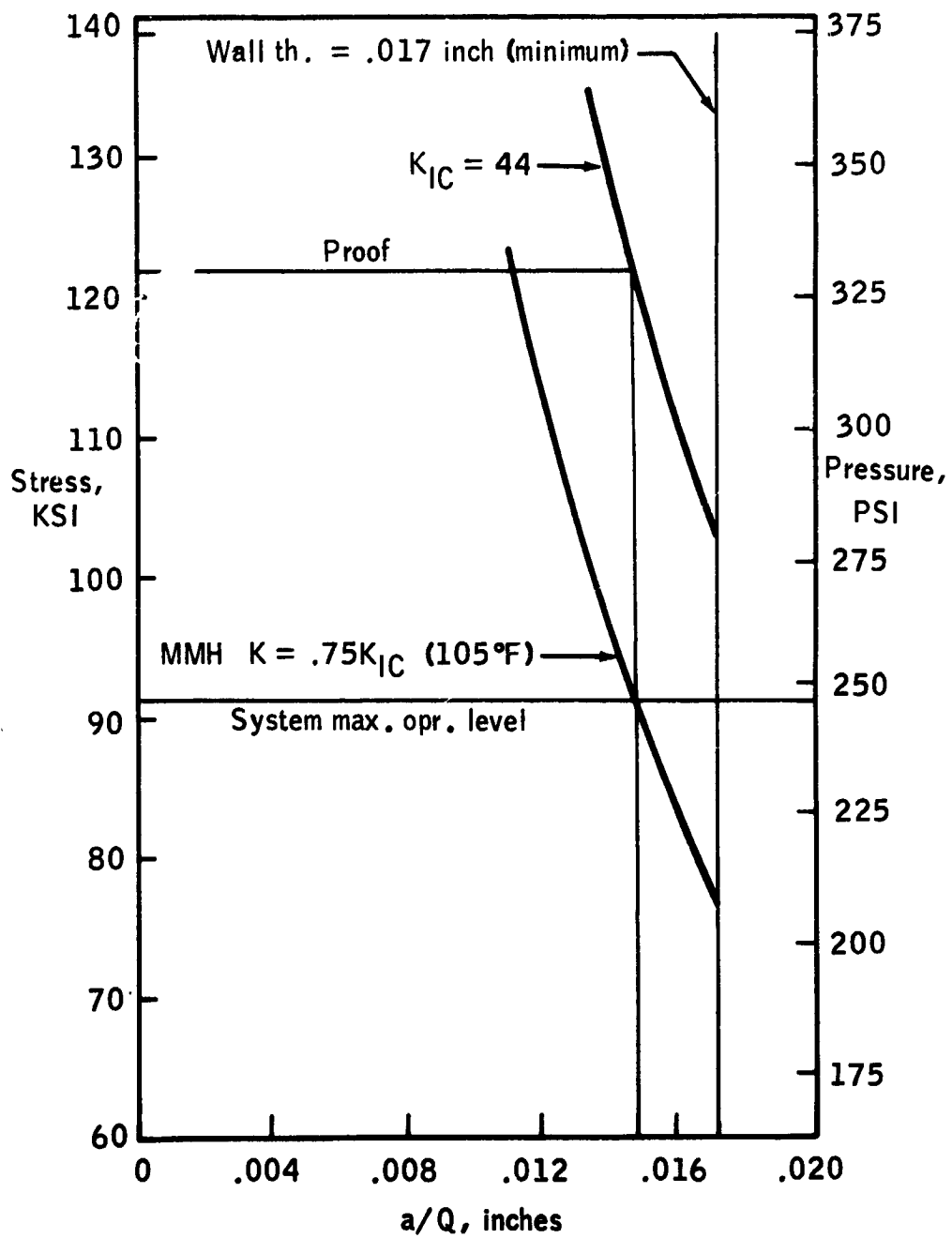


Figure 14. - Analysis of SM RCS fuel vessel proof test and operating conditions.

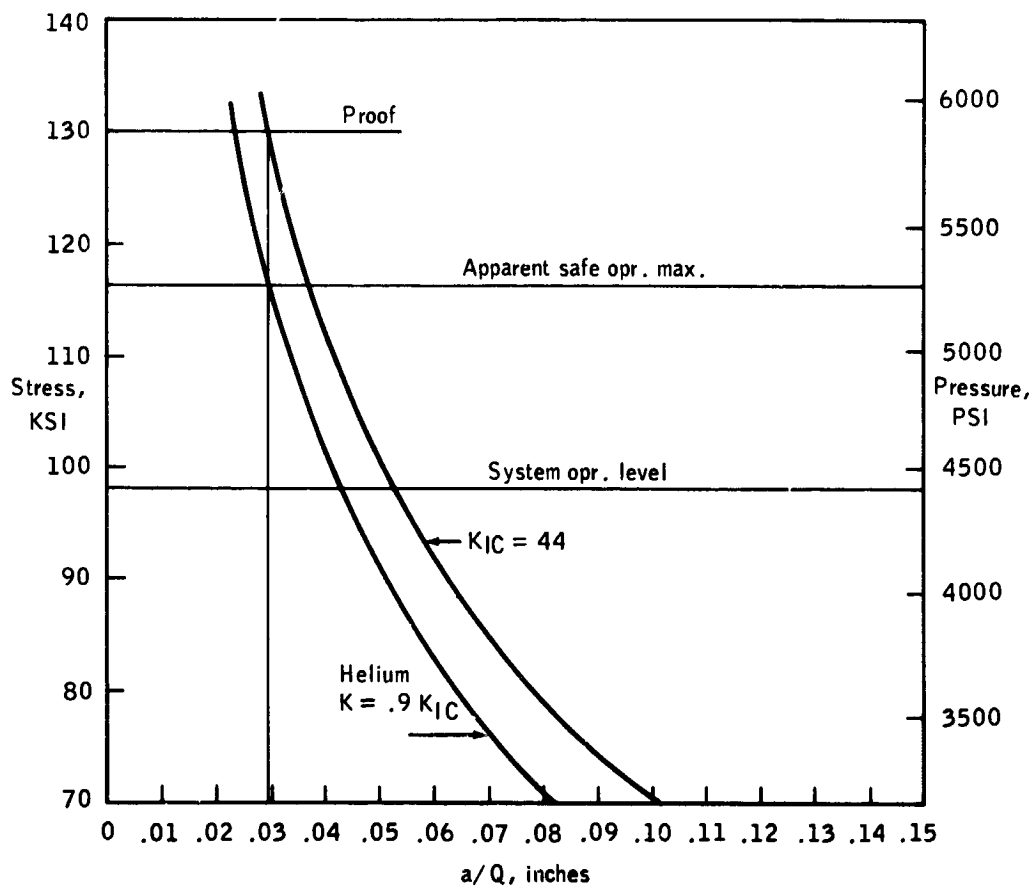


FIGURE 15. - Analysis of SPS helium vessel wall proof test and operating conditions.

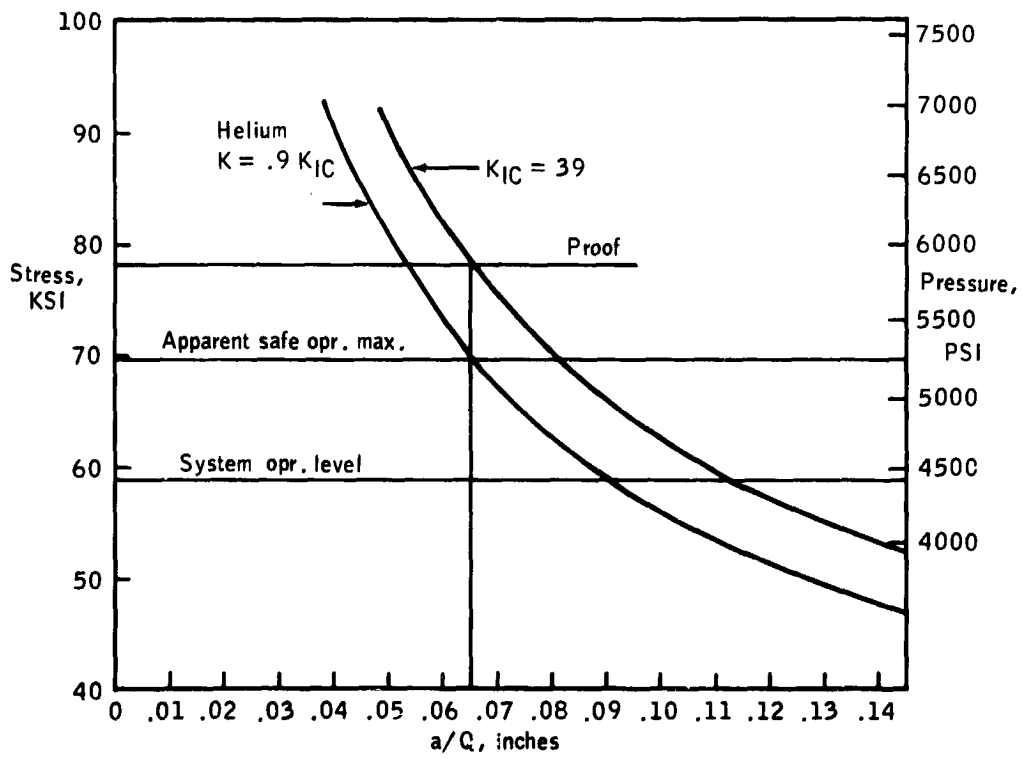


Figure 16. - Analysis of SPS helium vessel weld zone proof test and operating conditions.

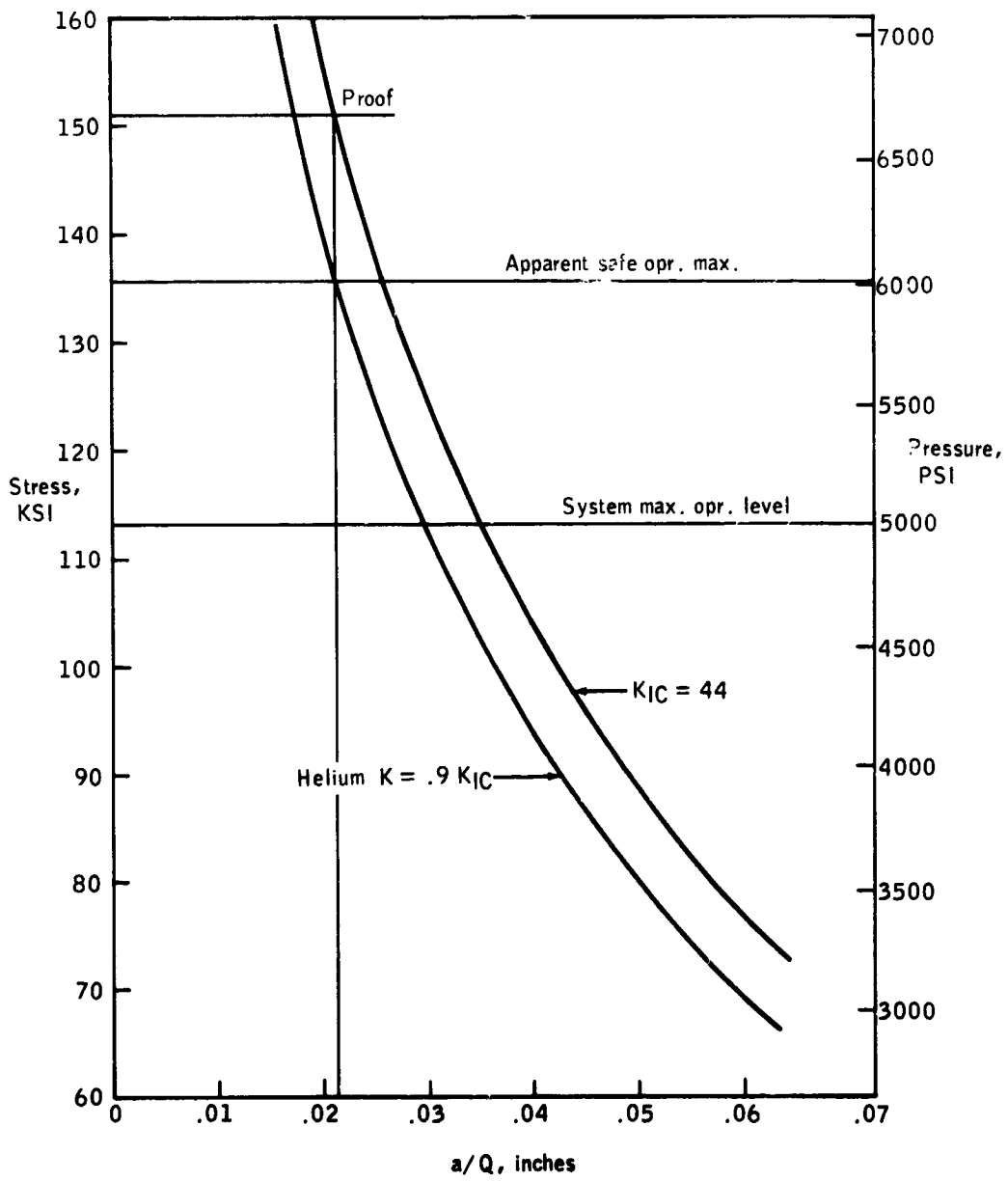


Figure 17.- Analysis of SM and CM RCS Helium vessels proof test and operating conditions.

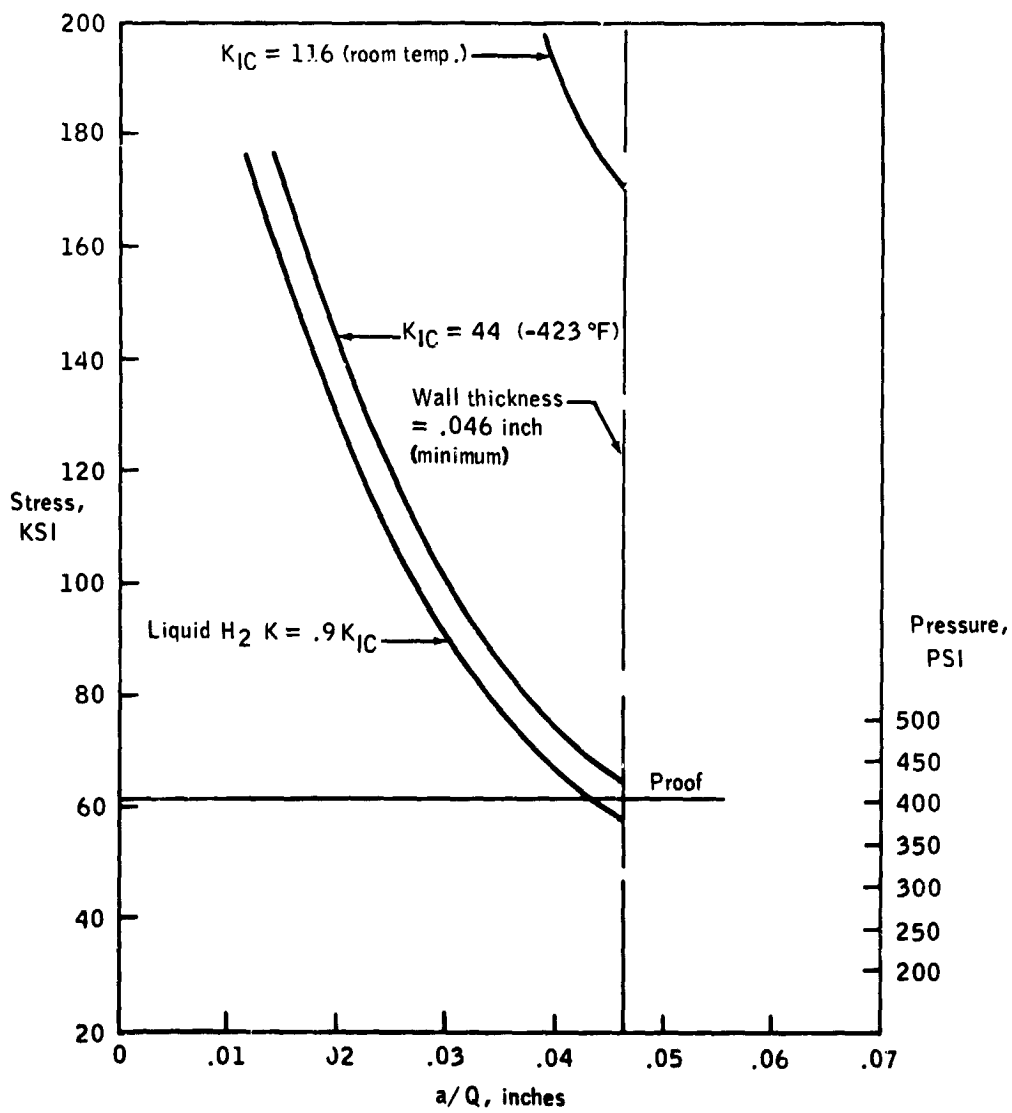


Figure 18. - Analysis of SM liquid hydrogen vessel proof test and operating conditions.

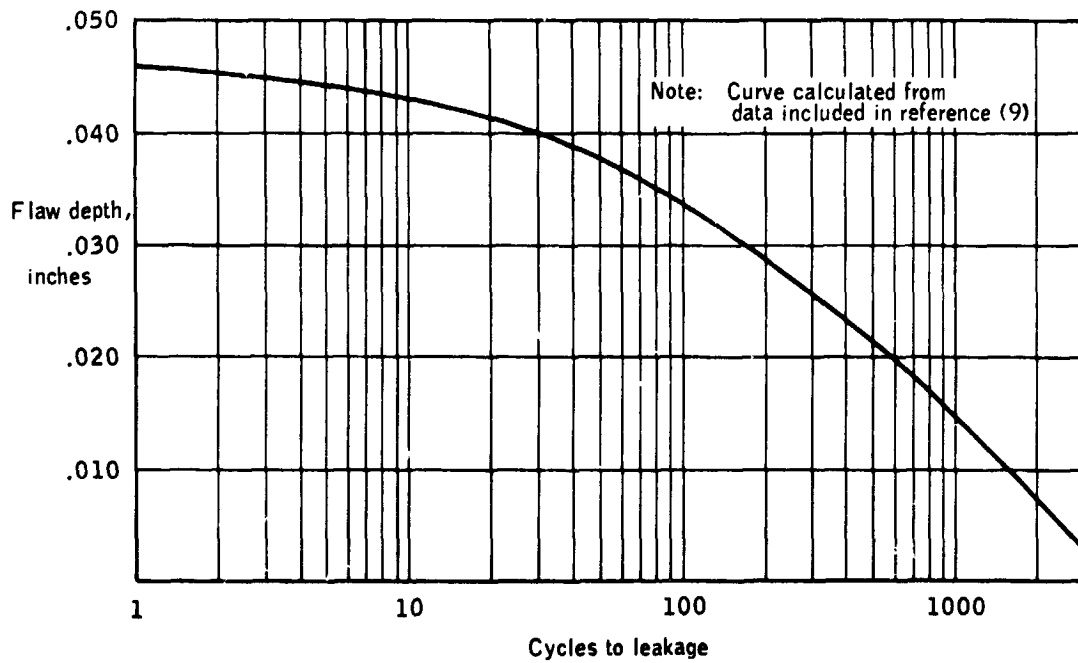


Figure 19. - Fatigue crack growth data for Titanium 5Al-2.5Sn ELI alloy at -423°F.

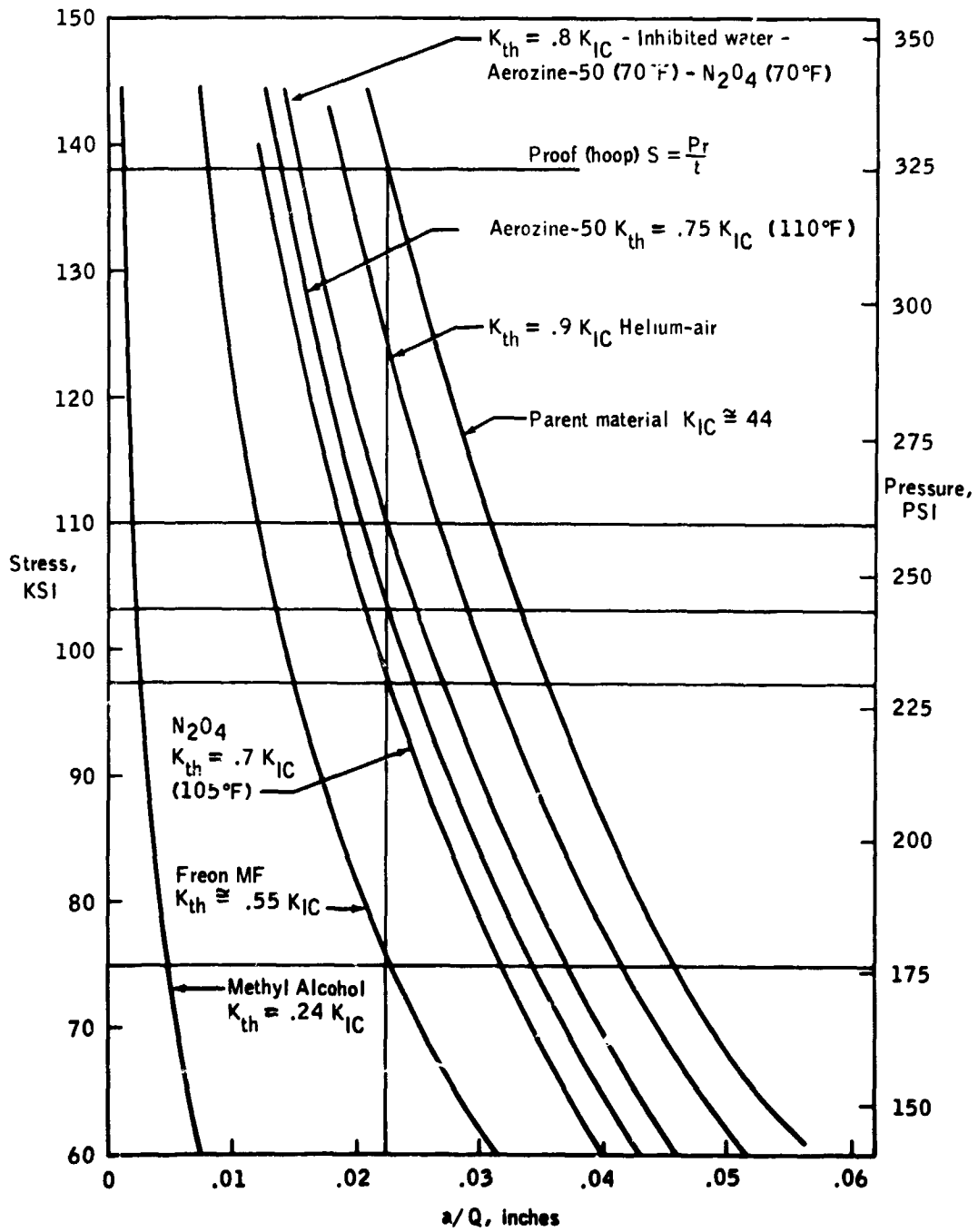


Figure 20. - Analysis of SPS oxidizer vessel cylinder roof test and environment thresholds.

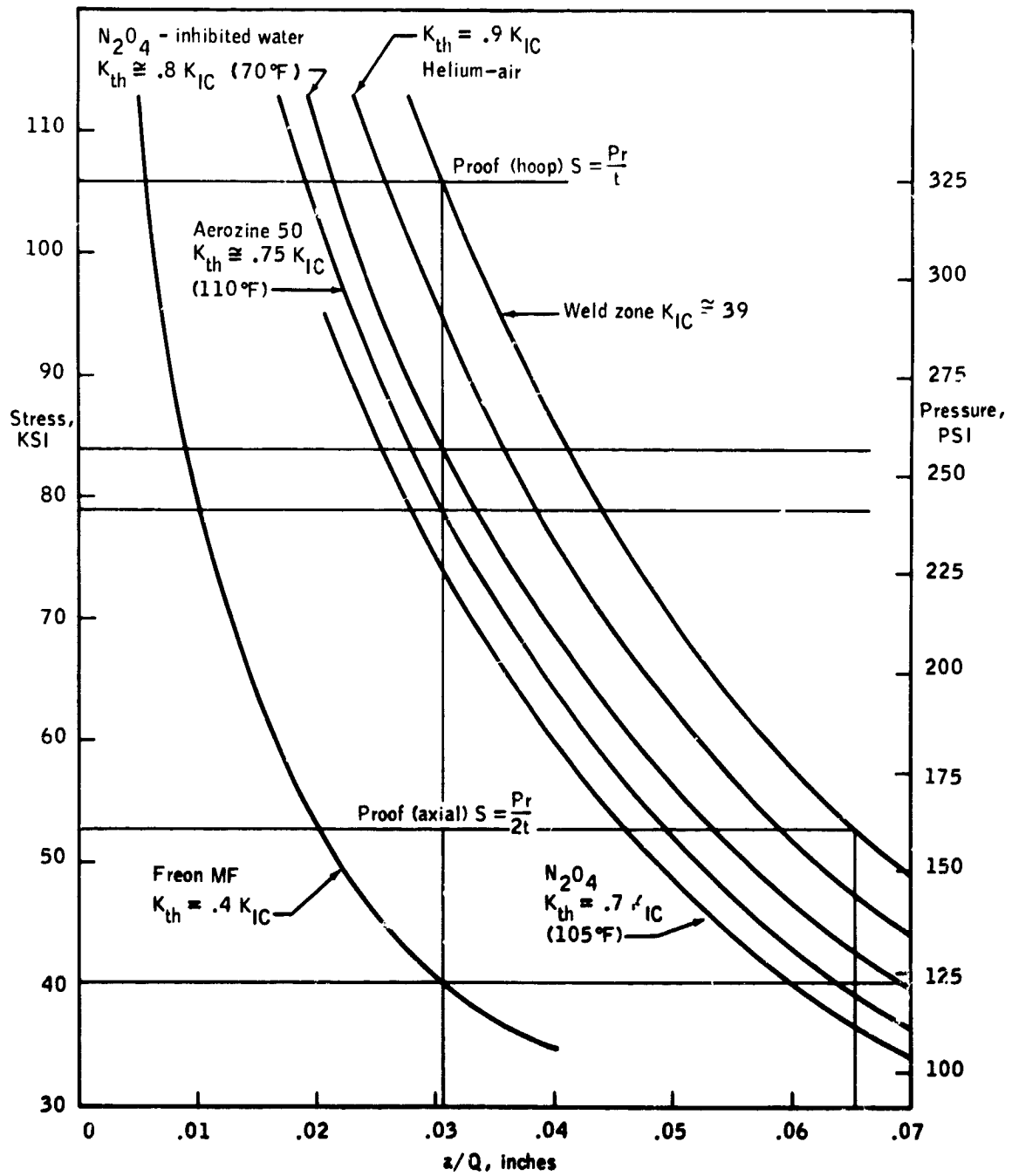


Figure 21. - Analysis of SPS oxidizer vessel weld zone proof test and environment thresholds.

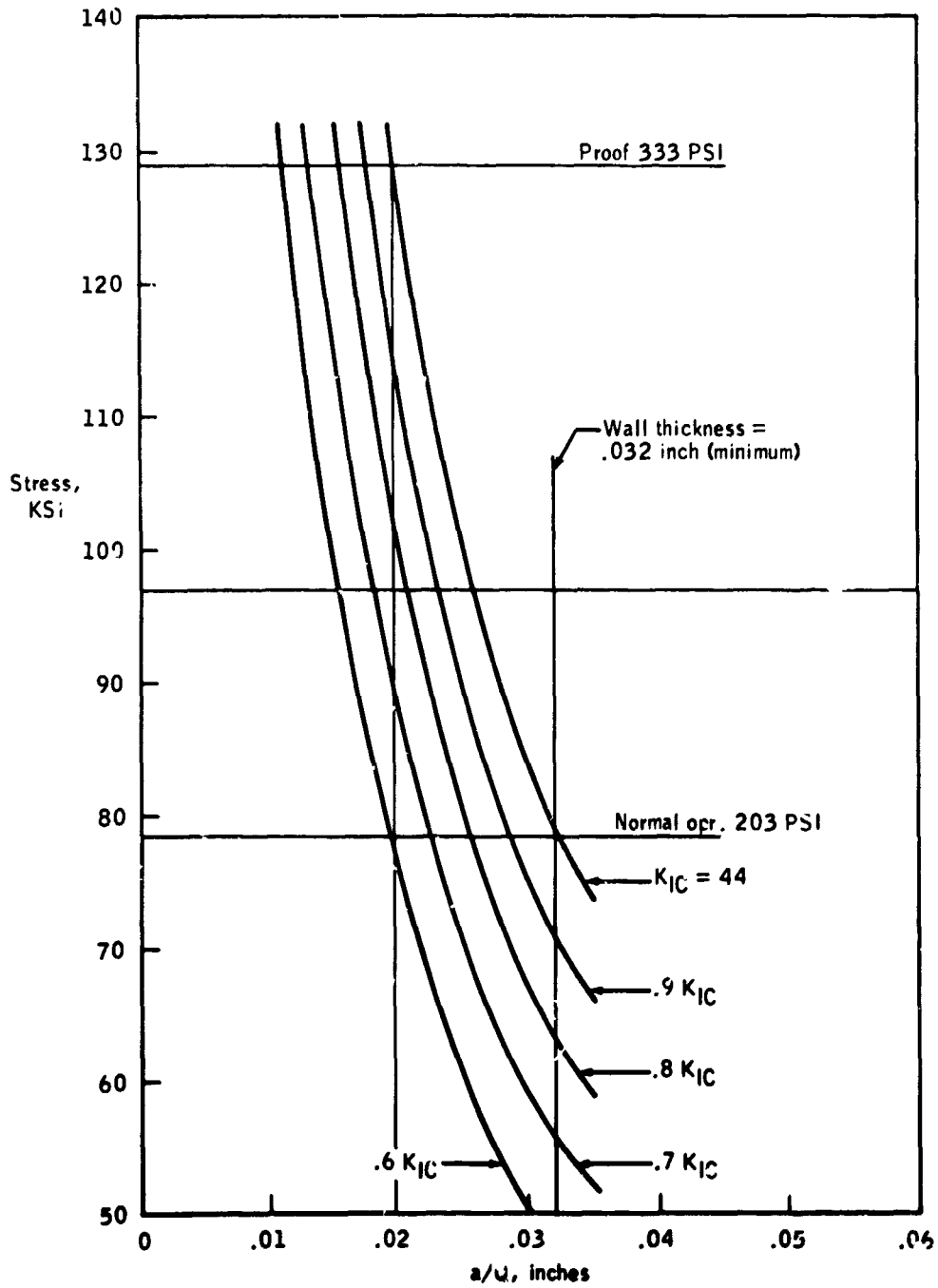


Figure 1A. - Lunar module ascent propellant vessels membrane. Proof test and threshold curves.

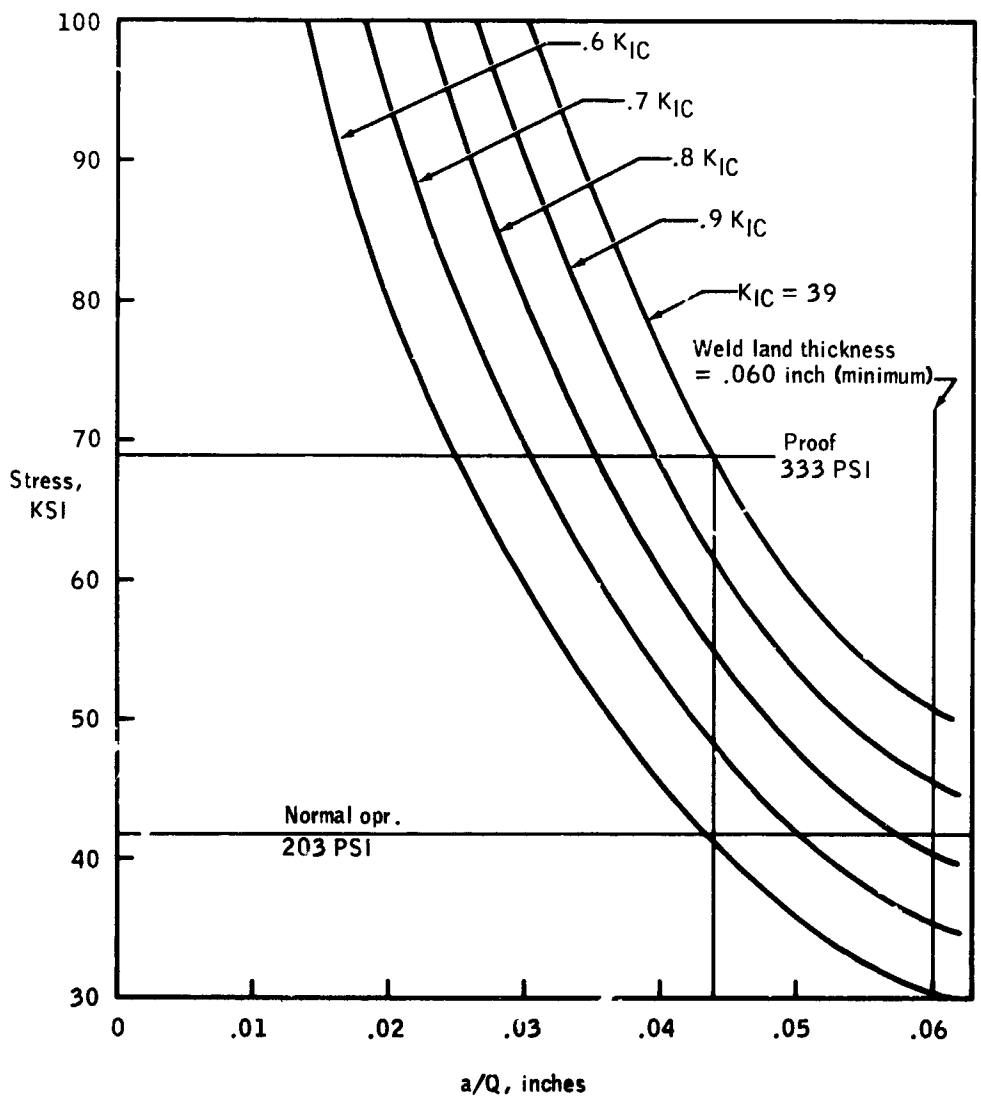


Figure 2A. - Lunar module ascent propellant vessels weld. Proof test and threshold curves.

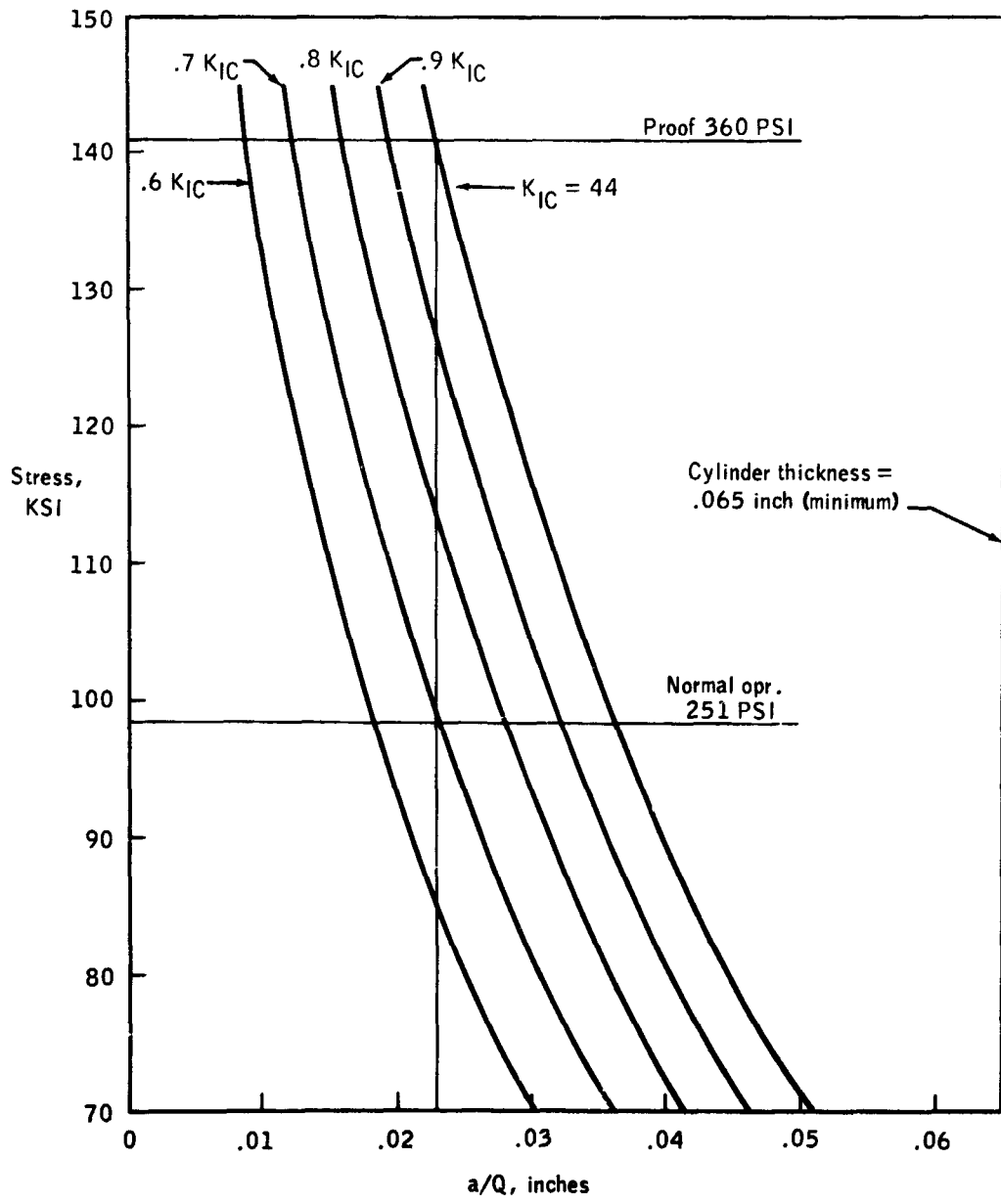


Figure 3A. - Lunar module descent propellant vessels membrane. Proof test and threshold curves.

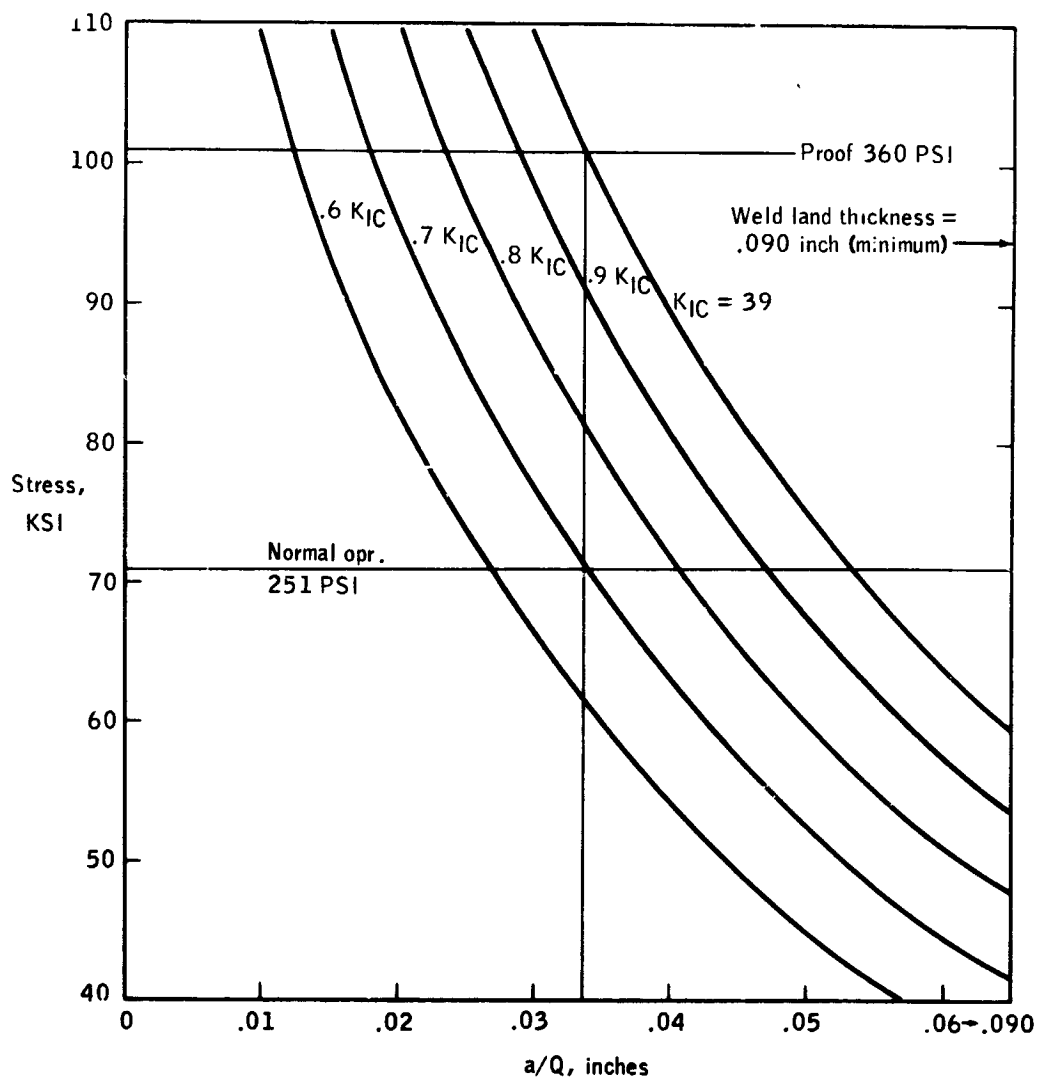


Figure 4A. - Lunar module descent propellant vessels weld. Proof test and threshold curves.